

Atmosphere

Volume 15 Number 1 1977

Canadian Meteorological Society
Société Météorologique du Canada

Atmosphere

Volume 15 Number 1 1977

Contents

1

Direct Simulation of Convective Adjustment and
Other Ensemble Effects

David E. Dietrich

19

Experiments with a Polar Filter and a One-Dimensional
Semi-Implicit Algorithm

Philip E. Merilees, Pierre Ducharme, and Ghislain Jacques

33

An Alberta Study to Objectively Measure Hailfall Intensity

G.S. Strong and E.P. Lozowski

54

Notes and Correspondence

57

Book Reviews

58

Announcements

59-60

Formule d'adhésion/Membership Application Form

ISSN 0004-6973

Canadian Meteorological Society
Société Météorologique du Canada

Direct Simulation of Convective Adjustment and Other Ensemble Effects

David E. Dietrich
JAYCOR, 205 South Whiting Street,
Alexandria, Virginia 22304

[Manuscript received 29 April 1976, in revised form 5 October 1976]

ABSTRACT

Convective adjustment is studied using results from a two-dimensional numerical model (of a baroclinic, dry, rotating fluid) that, in contrast to parameterization approaches, uses the *full dynamic equations in spectral form* to determine interactions among large-scale quasi-geostrophic waves and small-scale eddy ensembles. Both the large-scale and the small-scale eddies result from *physical* instabilities. The spectral formulation has desirable energy propagation and conservation properties, and also has the advantage (not implemented in this early study) of allowing one to determine interactions between different scale eddies

without having to represent intermediate scale eddies. The primary results are that: (i) there is a clear spectral gap in interactions affecting large-scale eddies and (ii) the large-scale vertical heat transport by the small-scale eddy ensembles varies significantly with time. This variation appears at least partly associated with ensemble group velocities in a *space-varying* large-scale environment, rather than with time variations of the large-scale environment (as would be consistent with the parameterization assumption that large-scale fields determine nonlinear transports by unresolved eddies).

1 Introduction

It is well established that ensembles of small-scale atmospheric eddies affect large-scale atmospheric eddies (scales of 1000 km or more) and vice-versa. The primary mechanisms for the former processes are vertical transports of heat and momentum and conversion between latent and sensible heat. The large-scale eddies, in turn, modulate the small-scale eddies. CISK is a widely discussed example of an important scale interaction (Charney and Eliassen, 1964; Ogura, 1964; Ooyama, 1964; Bates, 1973; Lindzen, 1974).

These phenomena have important nonlinear aspects and are not understood in detail. Recent power spectrum measurements (Högström and Högström, 1975) have shed new light on the mechanisms; the implied gap in the energy spectrum suggests that "nonlocal" spectral interactions discussed in this section are very active and may be predominant. The current AMTEX data (Ninomiya, 1975) are being gathered to gain more quantitative information on the primary

mechanisms. The main practical requirements are quantitative relations between large-scale vertical transports of heat and momentum and latent heat release (dependent variables), and large-scale fields (independent variables). Extensive and accurate measurements are required. I believe the present numerical approach can complement such data, and yield a detailed picture which is difficult to obtain purely from observational data.

Previous numerical studies have been primarily concerned with convection in a mesoscale environment and have focused on the detailed structure and physics of individual convection eddies and/or on the mesoscale space-averaged transport properties. The present study is more concerned with how an *ensemble* of small-scale convective eddies is modulated in space and time by nonlinear interaction with time-dependent large-scale eddies. The basic requirements for such a numerical study are that both long, quasi-hydrostatic, quasi-geostrophic waves (resulting from baroclinic instability), and short, non-hydrostatic, nonlinear waves (resulting from static and boundary-layer shear-induced instabilities) be modelled explicitly. The small-scale eddies must be determined by the Navier-Stokes equations, rather than by some greatly simplified physical relationships; the goal is to *improve* such parameterization relations. A spectral approach is very attractive, since it would: (i) allow one to represent widely separated scales of motion without having to represent intermediate scales, by using a “spectral gap” model; (ii) eliminate small-scale group velocity errors associated with linear phase speed errors. The latter are important because group velocity is a fundamental parameter in determining small-scale ensemble interactions with large-scale eddies (Dietrich, et al., 1975). Finite difference truncation error leads to large phase and group velocity errors in the small-scale flow components. It would (iii) allow conservation of energy in triad interactions between a long wave and two short waves, which is important in describing instability phenomena. Finite difference approaches do not allow such triad energy conservation because of the “aliasing” effects of truncation error. It would (iv) facilitate the quantitative description of the interactions among various scales of motion. It would (v) allow one to eliminate numerically troublesome high-frequency phenomena that do not influence large-scale eddies (Dietrich et al., 1975). Thus, a spectral approach is used in the present model, as described below.

A primary question is whether the most active interactions occur among widely separated scales of motion, with wave lengths differing by a factor of ten or more, or among relatively close scales of motion. The former interactions are spectrally “nonlocal” and characterize instability phenomena; the latter are “local” and characterize cascade phenomena. Since instability phenomena are such that the small-scale eddies have small time scales compared to the associated large-scale flow, it is reasonable to assume that the *effect* of the small-scale eddies on the large-scale eddies is in a kind of quasi-equilibrium dictated by the instantaneous state (and, perhaps, the very recent history) of the large-scale eddies. This is the basic assumption of parameterization methods, which specify the *effects* of unresolved small-scale eddies on the

resolved eddies in terms of the instantaneous state of the resolved eddies; the assumption is certainly valid for molecular transport phenomena, where the appropriate parameterization is simple diffusion; it is not yet clear just how well the assumption applies to large-scale effects of macroscopic mesoscale atmospheric eddies, but the assumption should be more nearly valid for instability phenomena than for cascade phenomena. This suggests that the large-scale components of flows with one or more “spectral gaps” (i.e. with widely separated bands in wave number space of actively interacting wave numbers, and relatively inactive gaps between the bands) are probably more predictable than those in “turbulent” flows dominated by cascade phenomena. Thus, the primary question of whether the dominant interactions are nonlocal is relevant to atmospheric predictability. Also, if they are nonlocal (other than the interactions among the energetic long waves), then application of a spectral gap approach might be possible in large-scale atmospheric forecast models. Finally, it should be noted that the significance of interactions affecting a large-scale wave depends on *whether they have a significant mean value on the time scale of the large-scale wave*; thus, the relative impact of “nonlocal” interactions which tend to remain in a given phase relative to the large-scale wave may be larger than instantaneous interactions may suggest.

2 The physical system

The physical system is a viscous, thermally conducting, Boussinesq, incompressible fluid between two rotating horizontal plates. The only y (latitudinal) dependence is an imposed linear temperature variation that is constant in space and time. (Temperature influences flow only through its *gradients*, so one can assume no further y -dependence.) Curvature terms are ignored. With appropriate choice of model parameters, eddies corresponding to baroclinic, static, and boundary-layer shear-induced instability occur. The baroclinic eddies are generally of much larger scale than the latter two types. The eddies equilibrate by: (i) vertical transports of heat and momentum; (ii) non-geostrophic cascade of energy into dissipative, smaller horizontal-scale eddies; (iii) direct transfer of energy to much smaller-scale eddies. Although all eddies are affected by all three mechanisms, the baroclinically and statically unstable eddies of interest equilibrate mainly by vertical transports of heat, and the shear-induced eddies equilibrate mainly by vertical transports of momentum and by non-geostrophic energy cascade. In the atmosphere, there is, in addition to these mechanisms, quasi-geostrophic cascade of energy to smaller scales (Charney, 1971), and latitudinal transports of heat and momentum. The quasi-geostrophic cascade mechanism is associated with terms of the form $u'\partial(q')/\partial x$, where q is any variable whose tendency is relevant and the primes indicate eddy quantities (deviations from zonal averages). This mechanism is represented only by ageostrophic u' in the present model. The latitudinal transport mechanism associated with equilibration requires latitudinal variations not included in the present two-dimensional formulation. A quasi-geostrophic cascade mechanism could be included in a two-dimensional model by imposing an

x -variation of the latitudinal temperature gradient at the surface, such as that associated with land–sea differences, and by including an appropriate predictive equation for the latitudinal temperature gradient as well as for the temperature. However, the quasi-geostrophic cascade phenomenon in such a model would be associated with moderate large-scale divergence, while the atmosphere has important quasi-geostrophic cascade effects associated with the nondivergent component of horizontal flow. Thus, the importance of the quasi-geostrophic cascade mechanism in such a two-dimensional model may be different from its importance in the atmosphere. Williams (1967) uses a model similar to the present one, to study important non-geostrophic effects in high-Rossby-number late stages of frontal development. As he notes, nonlinear quasi-geostrophic effects are associated with the early low- and moderate-Rossby-number frontal development.

Using this simple model, some of the primary mechanisms of interest can be studied with greatly reduced cost and effort, while setting the groundwork for more efficient and more elaborate models (perhaps using a “spectral gap” approach). A specific relevant question is: just how complicated must the parameterization be in order to achieve acceptable representation of large-scale effects of small-scale eddies? If a very complicated scheme is necessary for accurate parameterization of the results of this model, then even more complicated schemes are probably required for the atmospheric interactions, and the use of a “spectral gap” model might prove more efficient in such a case.

The mathematical formulation of the laws governing the present simplified physical system is:

$$\left(\frac{d}{dt} + f\mathbf{k} \times\right)\mathbf{V} + \alpha_0\nabla\phi - g\beta\epsilon z\mathbf{j} - g\beta\hat{T}\mathbf{k} = \nu_{ex}\mathbf{V}_{xx} + \nu_{ez}\mathbf{V}_{zz}, \quad (\text{a})$$

$$\frac{d\hat{T}}{dt} - \epsilon\nu = \kappa_{ex}\hat{T}_{xx} + \kappa_{ez}\hat{T}_{zz}, \quad (\text{b}) \quad (1)$$

$$\nabla \cdot \mathbf{V} = 0, \quad (\text{c})$$

where

$$\hat{T} = \hat{T}(x, z, t) = T(x, y, z, t) + \epsilon y$$

$$\frac{d}{dt} = \frac{\partial}{\partial t} + (\mathbf{V} \cdot \nabla)$$

$$\mathbf{V} = u\mathbf{i} + v\mathbf{j} + w\mathbf{k}$$

$$\nabla = \mathbf{i} \frac{\partial}{\partial x} + \mathbf{k} \frac{\partial}{\partial z}$$

$$p = \phi - (g\beta\epsilon/\alpha_0)yz$$

p is the usual non-hydrostatic pressure component, ϵ is the imposed constant latitudinal temperature gradient, β is a coefficient of thermal expansion, α_0 is the mean specific volume, which is assumed constant except in buoyancy terms,

and ν_{ex} , ν_{ez} , κ_{ex} , and κ_{ez} are horizontal and vertical-eddy transfer coefficients which are used to crudely parameterize even smaller-scale eddies than those explicitly resolved by the model. The model boundary conditions are:

$$\begin{aligned} \mathbf{V} &= 0 \text{ at } z = 0 \text{ and at } z = H, \\ \hat{T} &= 0 \text{ at } z = 0, \hat{T} = \sigma H \text{ at } z = H \end{aligned} \quad (2)$$

The flow is assumed periodic in x with a specified fundamental wave length.

3 The numerical formulation and procedure

For the reasons noted in the Introduction, the horizontal (x) variations of the fields are represented by Fourier series. In order to improve computational efficiency when high horizontal resolution is used, multiplications are performed in real space (using a fast Fourier transform algorithm to map between real and Fourier amplitude space). To assure that the products are non-aliased (and, thus, energy conserving), the number of real points used is *twice* the number of real Fourier amplitudes.¹ To facilitate accurate boundary-layer description while restricting the vertical resolution to *about* ten levels, a stretched vertical coordinate (z') is introduced:

$$z' = A \tan \left\{ B \left(z - \frac{H}{2} \right) \right\} \quad (3)$$

where A is a normalizing coefficient and B is chosen such that roughly $\frac{1}{4}$ of the total change of z' occurs in the Ekman layer associated with the vertical eddy transfer coefficient ν_{ez} . A staggered grid (Williams, 1969), uniform in z' , is used. Vertical derivatives are calculated using

$$\frac{\partial(\)}{\partial z} \Big|_{z'=z'_i} = B \left(A + \frac{(z'_i)^2}{A} \right) \frac{\partial(\)}{\partial z'} \Big|_{z'=z'_i} \doteq B \left(A + \frac{(z'_i)^2}{A} \right) \frac{(\)_{i+\frac{1}{2}} - (\)_{i-\frac{1}{2}}}{\Delta z'} \quad (4)$$

Higher order derivatives are approximated using successive applications of the first *difference* approximation, thus conserving flux quantities. *All* linear terms are treated implicitly in time, using a trapezoidal (Crank-Nicolson) scheme. The nonlinear terms are treated using a forward time difference followed by a trapezoidal corrector. This allows a time step² six times greater than the Adams-Bashforth treatment of the nonlinear terms, with no significant increase in computation or storage. If all terms were treated implicitly using the trapezoidal rule, this would correspond to the numerical formulation given by Dietrich (1975) which conserves energy exactly in both space and time. The coupled linear implicit difference equations in z' are solved using a one-dimensional special case of the scheme described by Dietrich (1975).

¹Non-aliased results can be obtained using a number of real points one and one-half times the number of Fourier amplitudes, thereby saving time over the algorithm used.

²The model time step used for the results discussed below is about one-half the vertical advection CFL during the most vigorous convection. This vigorous convection follows a period during which the vertical heat transport by the convective ensemble increases about 30 per cent per model time step.

The time marching is divided into three parts: (i) the wave-absent equations with initial conditions independent of x are integrated to a quasi-steady state; (ii) a few long waves are introduced through arbitrary temperature perturbations and low resolution equations are integrated until the waves are quasi-equilibrated; (iii) the high resolution equations are then integrated in time until quasi-equilibration is again achieved. The nonlinear terms drop identically from the equations for stage (i), since $w = 0$ and $\partial/\partial x = 0$.

Considerable savings are achieved by separating stage (iii), since a shorter time step *and* more computation per time step is required than in (i) or (ii). However, by using a more implicit vertical advection scheme (such as advocated by Dietrich et al., 1975), by subtracting out numerically troublesome high-frequency horizontally propagating modes (as described by Dietrich et al., 1975), and by utilizing a “spectral gap” approach advocated as here, it may be possible to greatly increase the computation efficiency in (iii), without significantly affecting the long-wave behaviour.

4 Results

Of primary interest in this study are high-resolution numerical experiments in which both large-scale quasi-geostrophic waves and small-scale convective boundary-layer eddies are resolved. However, several results from low resolution experiments are of interest as well.

a *Low Horizontal Resolution Cases* (With four or fewer waves)

In the second stage of the three-step time integration procedure described in Section 3, the longest represented wave (the fundamental Fourier mode) dominates the flow after sufficiently long time integration. Smaller-scale eddies are significant only when horizontal wavelengths comparable to the depth of the unstable boundary layer created by the large-scale flow are resolved in the third stage. Although the harmonics may temporarily dominate the flow because of their larger growth rates at the beginning of stage (ii), the fundamental continues to grow after the interior static stability increase caused by vertical eddy heat transport neutralizes the harmonics.³ Eventually, the harmonics decay and the fundamental equilibrates, with some energy cascade into the harmonics. Such energy cascade maintains the harmonics at a much lower energy level than they originally attained as unstable modes in the mean flow, since it relies on inefficient non-geostrophic cascade of energy. (The energy cascade is associated with nonlinear products of the relatively small non-geostrophic part of the flow.) It should be noted that a sufficiently large increase of interior static stability implies destabilization of the boundary layers, since the upper and lower boundary temperatures are fixed in the present model. However, in the high-resolution results described below, the boundary-layer destabilization is due primarily to horizontal advection, not vertical heat transport.

A strong tendency for *steady* finite amplitude equilibration is found in low-resolution cases with Prandtl number, $Pr \equiv \nu_{ez}/\kappa_{ez}$, equal to one. For example,

³There is no beta-effect to stabilize long waves in the present model.

a case was run with $Pr = 1$, $Ro_T \equiv 2\pi(g\beta\epsilon H/f^2L) = 0.79$, and $Ek \equiv \nu_{cz}/fH^2 = 0.0005$, where Ro_T and Ek are thermal Rossby and Ekman numbers, and L is the fundamental wave length. *With two waves resolved* and 14 levels in a stretched vertical coordinate, the flow has a steady finite-amplitude equilibration. A similar case was run with ν_{cz} increased by a factor of ten, and all other parameters unchanged, so that $Ro_T = 0.79$, $Pr = 10$, and $Ek = 0.005$. In this case, the equilibration is very time dependent, with strong amplitude vacillation. These results appear superficially to be related to the diffusive destabilization phenomenon discussed by McIntyre (1968); however, his background flow does not have finite amplitude baroclinic waves which are present here.

b Detailed Results from a Case with High Resolution

A high resolution case was run with $Ro_T = 0.094$, $Pr = 10$, and $Ek = 0.0125$. Stage two of the integration resolved *four waves*. Stage three included *32 waves*, so the small-scale Rossby number is about 3. The small-scale horizontal wavelength is about twice the Ekman layer depth based on Ek . The vertical resolution was eleven levels in a continuously stretched vertical coordinate that magnifies boundary layer regions. The finite amplitude flow at the end of stage two is shown in Fig. 1(a). At the beginning of stage three, the newly resolved small-scale eddies are in a statically unstable large-scale environment, and the small-scale ensemble grows exponentially. The flow near the time of maximum small-scale activity is shown in Fig. 1(b). Fig. 2 shows the extremely rapid growth of the small-scale eddies (the e -folding time of the heat transport by the convective ensemble is about one model hour) during the early growth period. Figs 1(c) and 1(d) show the flow at times later in the stage three integrations.

Fig. 2 reveals a consistent relation between the large-scale vertical heat transport by the small-scale convective ensemble and large-scale flow parameters. Both the mean and wave number one components of the heat transport (curves E and F of Fig. 2) tend to grow when the boundary layer is relatively unstable (which is reflected by curves A and B being close together and C and D far apart⁴). This clear relation *suggests* that accurate parameterization may be possible in the present model with relatively simple parameterization relations. This may not be true for cases in which the convective heat transport has a more significant effect on the large-scale flow than in the present case. It is expected that, in the atmosphere, convective latent heat transport and release has a considerably more important effect than the sensible heat transport has in these results from the present dry model.

Curves E and F in Fig. 2 show the ensemble heat transport varying by about a factor of two even after the large initial adjustment. The dominant time scale is about one model day. The time dependence of the mean heat transport by a given wave number is even stronger, as suggested by the behaviour of wave numbers 23 and 24, shown in Fig. 3.

⁴The fact that curves C and D being far apart reflects an unstable boundary layer is related to the facts that the phase of the wave number one temperature field is nearly independent of height, and the amplitude increases toward mid-depth (see Fig. 1).

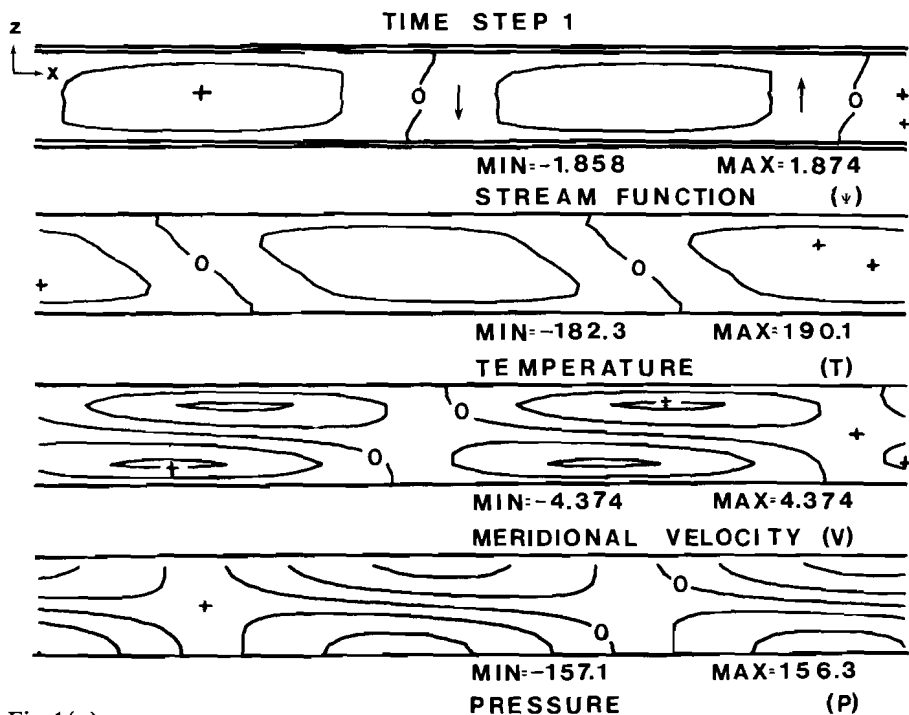


Fig. 1(a)

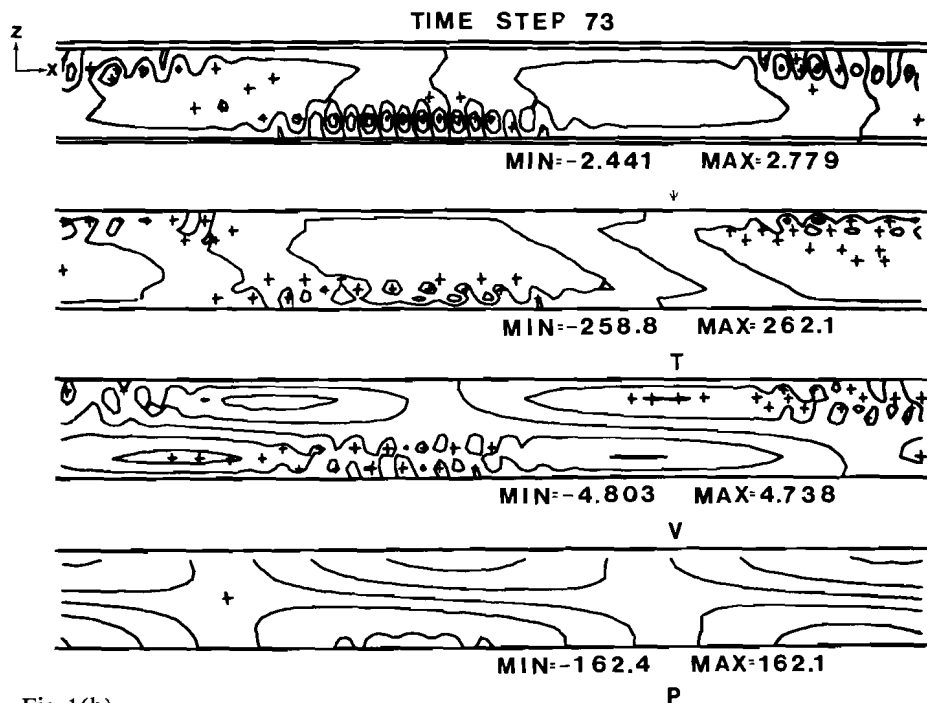


Fig. 1(b)

Fig. 1 Contour diagrams in $x - z$ planes showing eddy flow at time steps 1, 73, 97, and 177 of the stage-three (with 32 waves resolved) time integration. The time step is 1/96 day. Zonal (x) averages have been subtracted out to show eddy structure more clearly. The fields shown are: stream function for zonal overturnings (ψ);

TIME STEP 97

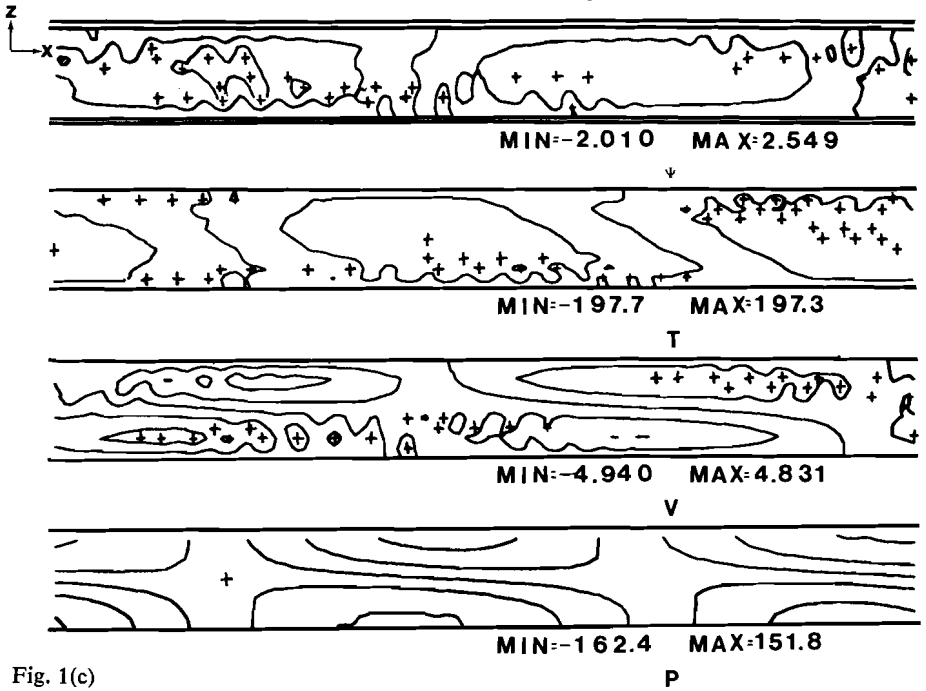


Fig. 1(c)

TIME STEP 177

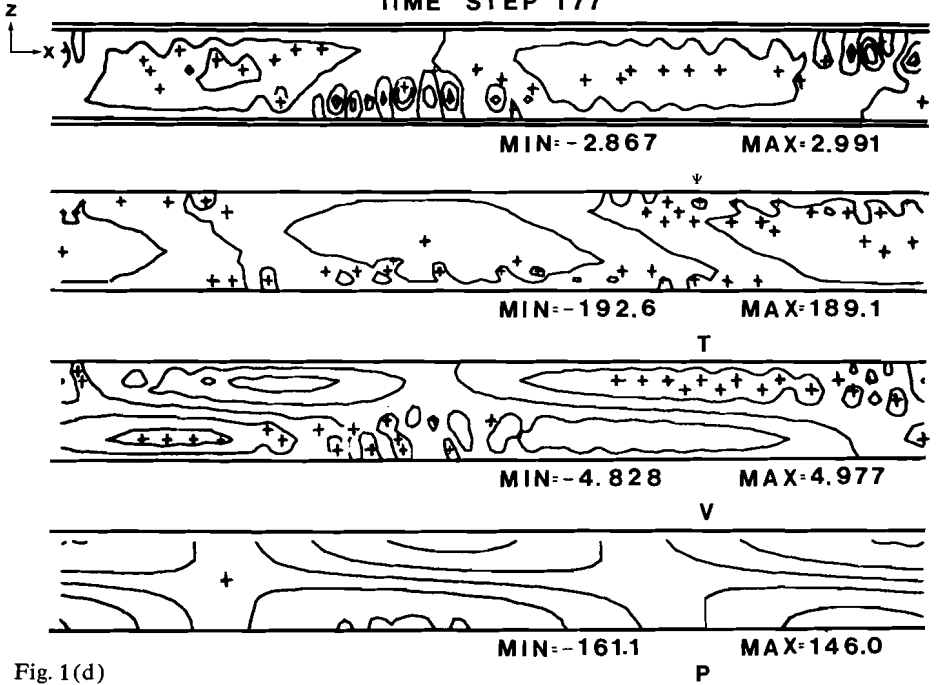


Fig. 1(d)

temperature (T); meridional velocity (v); and pressure (p). Local maxima are indicated by “+.” Ranges (minimums and maximums) are given. Zero contours are labelled. The arrows indicate flow direction. The vertical distance is stretched in the boundary layers.

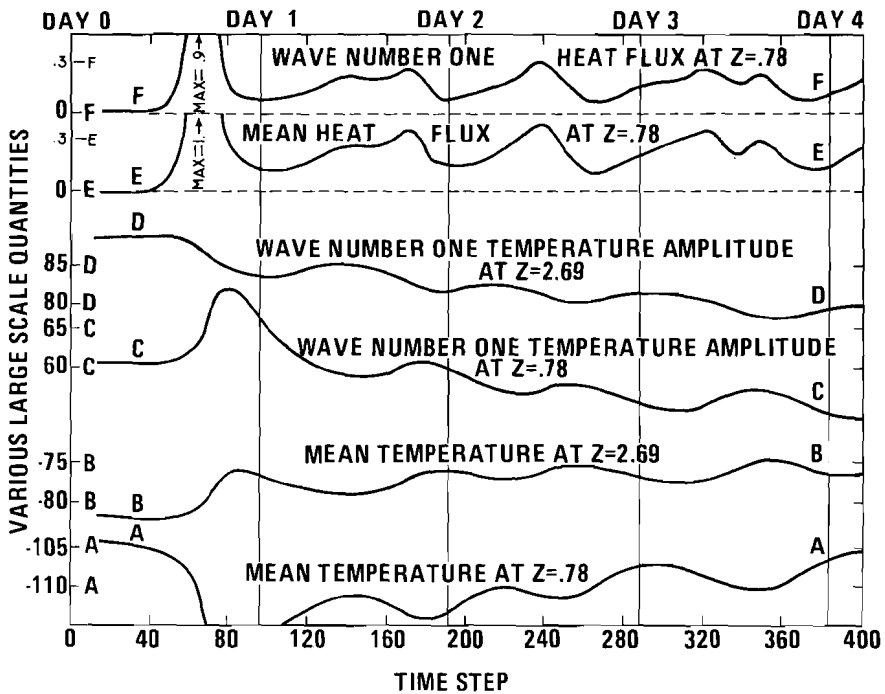


Fig. 2 Time dependence of six quantities. Abscissa is the stage three time step number. Ordinates corresponding to each of the six curves are indicated by letters A-F. The z -values given on each curve are model vertical coordinates using a vertical scale of ten units, with $z = 0$ at the bottom boundary. Curves E and F are total large-scale upward heat fluxes associated with the small-scale eddies; specifically,

$$\text{curve } E \propto \sum_{n=17}^{32} (W_n T_n^* + W_n^* T_n)$$

and

$$\text{curve } F \propto \left| \sum_{n=17}^{32} (W_n T_{n-1}^* + W_{n-1}^* T_n) \right|$$

where W_n and T_n are complex Fourier amplitudes of vertical velocity and temperature fields. Curves E and F are normalized relative to the maximum wave number 0 heat flux, which occurs at time step 68.

Arakawa and Schubert (1974) describe a nonlinear mechanism leading to what they call the "adjustment time scale," which could be associated with this time dependence. The mechanism involves the growth, nonlinear equilibration, and decay of convective ensembles in response to changes they induce in the large-scale static stability. Because of this nonlinearity, it may be difficult to explain the apparent natural period in the present results. In developing a nonlinear theory, one would have to consider changes in the large-scale "background" state, and the period would probably exhibit hysteresis effects depending on the initial state of the convective ensemble. Thus, it would be nice if a

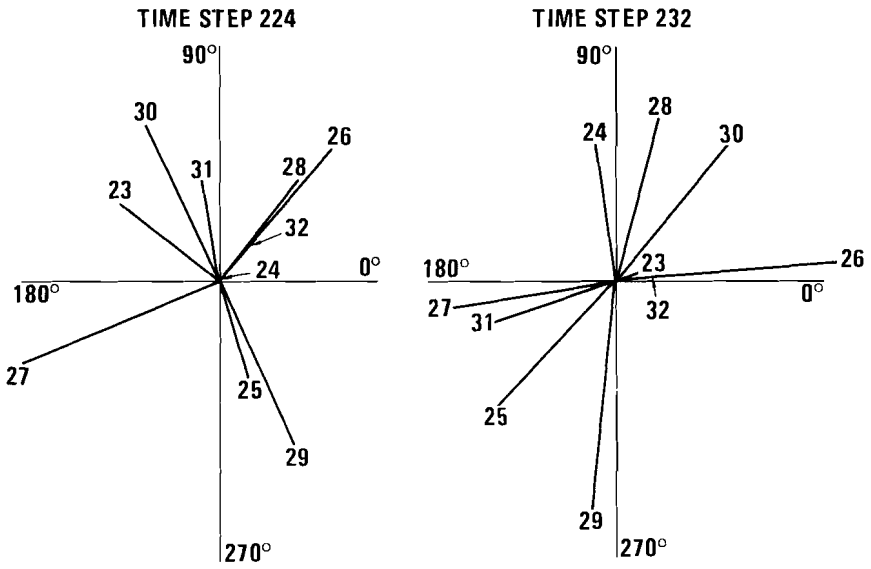


Fig. 3 Phase-plane diagrams showing amplitude and phase relations of most active small-scale eddy wave components (wave numbers 23–32) at time steps 224 and 232 of the stage-three time integration. Clockwise rotation of a vector from time step 224 to time step 232 corresponds to eastward phase propagation.

linear theory could explain the quasi-one-day oscillation in the present results and similar atmospheric phenomena.

The Arakawa-Schubert mechanism would be the likely explanation if there were significant one-day changes in the boundary-layer static instability (proportional to $\partial T/\partial z$). However, in the present results, both the mean and wave number one components of vertical temperature gradient vary by only about ± 5 per cent *even in the boundary layers*. There is no apparent mechanism by which such small variations could cause the much larger variations of convective ensemble flux in the boundary layers. (Evidence that the convective flux is not so sensitive to the large-scale flow was obtained from a run of the same case with all nonlinear interactions ignored except those involving or affecting the mean zonal flow. Although the static instability of the mean zonal flow is smaller by a factor of two than occurs under the cold dome of wave number one, the resulting mean zonal component of the convective ensemble heat flux is less by only a factor of two in this “reduced interaction” run.)

Thus, although there may be mechanisms for one-day oscillations of the large-scale flow (such as through nonlinear interactions with the convective ensemble or an inertia wave trapped in the statically unstable boundary layer), *the smallness of the time variations of the large-scale static stability in the present results suggests the explanation of the convective ensemble heat flux oscillation may not depend on such large-scale time variations.* A possible heuristic explanation not depending on such time dependence is as follows: the wave number one component heat transport is the net effect of contributions

from all wave number pairs of the form $(n, n + 1)$. Each pair corresponds to a given triad of interactions with a wave number one component. The phase velocities of the two small-scale components of each triad define a characteristic effective group velocity. This group velocity implies that small-scale energy in the interacting triad propagates relative to the long-wave environment. Since the large-scale static stability has a strong variation in its wave number one component, the small-scale energy is modulated by its interactions with the large scale as it propagates. The total wave number one heat transport, involving the net effect of all such triads, would also reflect such time dependence (but to a lesser degree, since the phase of the wave number one heat transport may vary from triad to triad). In the present problem, this time dependence is large at first, because the wave number one heat transport is nearly in phase for all pairs of small-scale wave numbers during the rapid initial growth of the small-scale convective band. Group velocity *variation* in the convective band gradually increases the variability of this phase, and the time dependence decreases.

This heuristic explanation assumes that most of the convective heat flux is associated with modes that have nearly the same (at least within a factor of two) group velocity. Otherwise, the time variation would be reduced to relatively small, nearly random fluctuations after the initial burst of activity. This raises the question of whether increasing the horizontal resolution would result in a wider wave number band of convective modes having significant heat transport and, if so, whether the group velocity would have large variation in the widened band. One way to reduce this possibility in the present simplified model is to use horizontal diffusion coefficients just large enough to significantly suppress wave numbers higher than the wave number most active in the absence of horizontal diffusion. Although the diffusion coefficients used in this study were chosen to be the right order of magnitude to significantly retard unresolved higher wave numbers, the high-resolution runs necessary to verify this choice have not yet been performed, because the high computation costs can be reduced by improved versions of the present model (as noted at the end of Section 3).

Whether this heuristic explanation offered for the present model time dependence may be relevant to atmospheric behaviour depends on whether there are significant cases (such as in east coast winter storms) where the convective modes transporting and releasing most of the latent heat have approximately uniform group velocity. If the active modes have a clear, characteristic horizontal scale, it is more likely that this will be true than if their energy is distributed over a wide range of scales.

The results shown in Fig. 3 indicate that the group velocities in the convective band are of the right order of magnitude to be consistent with this argument. That is, they are such that the energy propagates about one wave length (wave number one component) per model day. More convincing diagnostic evidence is difficult to obtain due to insufficient information on how the large scale modulates the small-scale convection in space *and* time. Separation of

dispersing gravity mode pairs having the same wave number⁵ might make the phase plane vectors more regular, but this has not yet been attempted. Theoretical analysis is very difficult, because of the strong vertical and horizontal variations of static stability, which has both positive and negative values in the convective boundary layer, and also because there might be no valid linearization of the problem. The detailed structure and boundary-layer depth probably affect the group velocity significantly.

The key point is that there is significant time variation of the convective heat transport that is *apparently* not due to time variations of the large-scale flow. That is, the time variation would probably occur even if the large-scale flow were exactly steady. Apparently, *space variations of the large-scale environment can significantly modulate the convective heat transport in time as well as in space, whether or not the large-scale flow is steady.* Besides indicating the potential complexity of convective heat transport parameterization, especially after rapid growth of a convective ensemble, this leads to the interesting question of what might happen if the conditions were such that the frequency of large-scale convective heating were close to the corresponding large-scale inertia-gravity frequency. A rapid growth of convective ensemble heat transport and latent heat release will itself trigger a *large-scale* inertia-gravity oscillation due to accompanying large-scale pressure changes. In a rapidly growing east coast winter storm, simple scaling considerations (Brunet, 1974) suggest that such an oscillation might make a significant contribution to large-scale convergence and associated precipitation. (These scaling considerations indicate that the pressure changes associated with realistic convective heat transport and latent heat release in a growing convective ensemble can induce significant oscillating, out-of-balance, large-scale vertical motions.) Brunet (1974) studied large-scale rainfall data from Hurricane Agnes and found evidence for such an oscillation, although the effect on large-scale precipitation is rather small in that case.

Associated with this small-scale convective time dependence is relatively small time variation (about ± 5 per cent) of large-scale fields, as shown by curves A, B, C, and D of Fig. 2. Convective ensemble heat transport and latent heat release may vary in a similar way in atmospheric disturbances with the ensemble changes being associated with relatively small changes of large-scale flow parameters. Note that such changes would be important in short-term convective precipitation probability forecasts.

As suggested by Fig. 3, the most active convection occurs in a band of wave numbers around wave number 27. However, wave number 32 grows the fastest *when interactions with only the mean zonal flow* are accounted for. This could be due to the unstable boundary-layer depth being less in the mean than it is under the "cold dome" of wave number one, thereby reducing the growth rates

⁵There are two primary gravity waves associated with each wave number, travelling in opposite directions.

of the lower wave numbers relative to wave number 32. This could also be due to wave number 32 (the highest represented wave number) having only one triad through which to obtain energy from wave number one, while the lower wave numbers have two. All waves have equal opportunity to interact with the mean flow.

The qualitative appearance of the fields shown in Fig. 1 suggests that there is relatively little activity in scales of motion between the large, quasi-geostrophic scale and the small, convective scale in the boundary layer. Fig. 4 confirms this quantitatively. Figs 4(a) and 4(b) are histograms revealing a strong gap in wave-number-band-averaged nonlinear heat transport interactions affecting large-scale temperature distribution. Fig. 4(c) shows a much less prominent gap in the temperature variance spectrum that, by itself, would suggest that the small-scale interactions are less important than indicated by Figs 4(a) and 4(b). However, the vertical velocity spectrum gives just the opposite picture, so that when one multiplies the RMS vertical velocity in each band by the corresponding RMS temperature, the resulting histogram is much more like Fig. 4(a) and Fig. 4(b) than is Fig. 4(c). Nevertheless, one should be very careful in making inferences from variance spectra alone, as these do not necessarily reflect the relative influence of different scales of motion on the large scales that are to be forecast. The reason is that phase relations, *averaged on the time scale of the large-scale eddies*, also influence the time-averaged vertical heat and momentum flux quantities.

The assumption of constant latitudinal temperature gradient used in the present model probably exaggerates the strength of the spectral gap indicated in Fig. 4, because this assumption eliminates the quasi-geostrophic cascade mechanism. Future studies should include this cascade mechanism, possibly within the framework of a two-dimensional model as mentioned in Section 2.

Finally, an interesting point about the structure of the convective eddies is that, while the vertical heat flux is predominantly upward, nonlinear inertia effects result in small downward flux on the interior side of unstable boundary layers. That is, fluid elements overshoot their equilibrium levels (where their temperature matches the large-scale environment temperature), so that upward moving fluid at the top of the lower boundary layer tends to be cooler than the average temperature at the same level. (This result has been observed by Deardorff et al., 1969, in laboratory experiments.) In fact, in the absence of dissipative effects and interaction with fluid at other levels, a fluid element would have its maximum vertical velocity at such an equilibrium level. Such downward heat transport cools the environment above the equilibrium level, thereby raising the equilibrium level for ensuing fluid elements. Thus, this nonlinear inertia effect deepens the convective boundary layer. It should also be noted that fluid deceleration above the equilibrium level generates gravity waves that can be important in momentum exchange with still higher levels. These nonlinear aspects of convective adjustment dynamics may be difficult to parameterize accurately in terms of large-scale flow parameters, although some schemes have been proposed for doing this (Deardorff et al., 1974). The

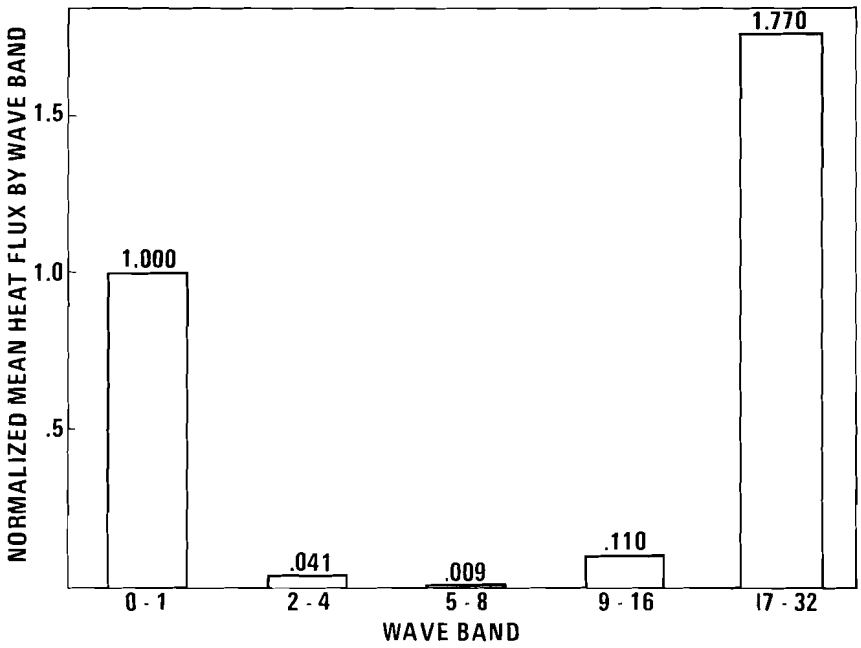


Fig. 4(a) Histogram showing time-averaged mean zonal heat transport by five individual bands of consecutive wave numbers. Horizontal scale of associated eddies decreases by about a factor of two for each bar proceeding left to right.

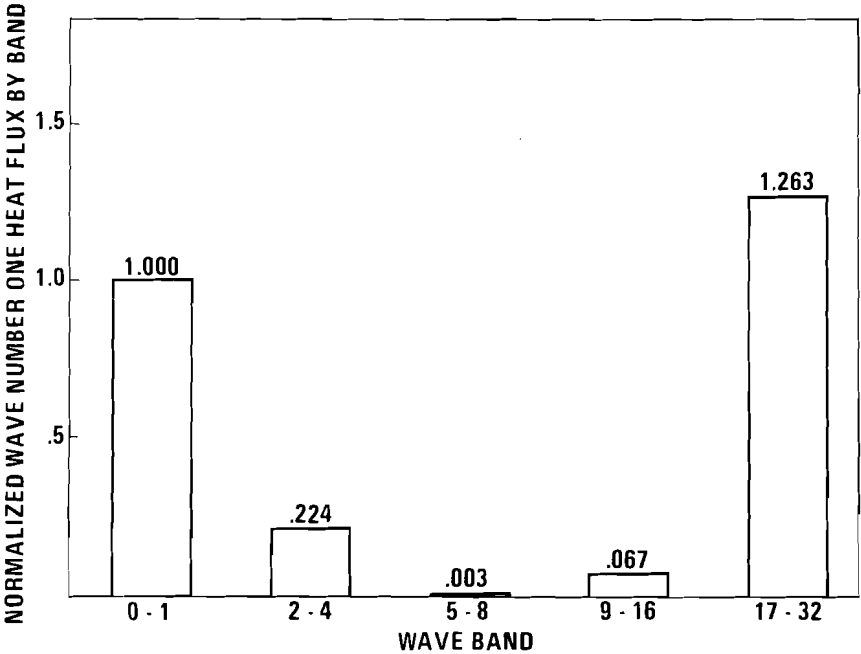


Fig. 4(b) Histogram showing amplitude of time-averaged wave number one heat transport by each of five bands of consecutive wave numbers.

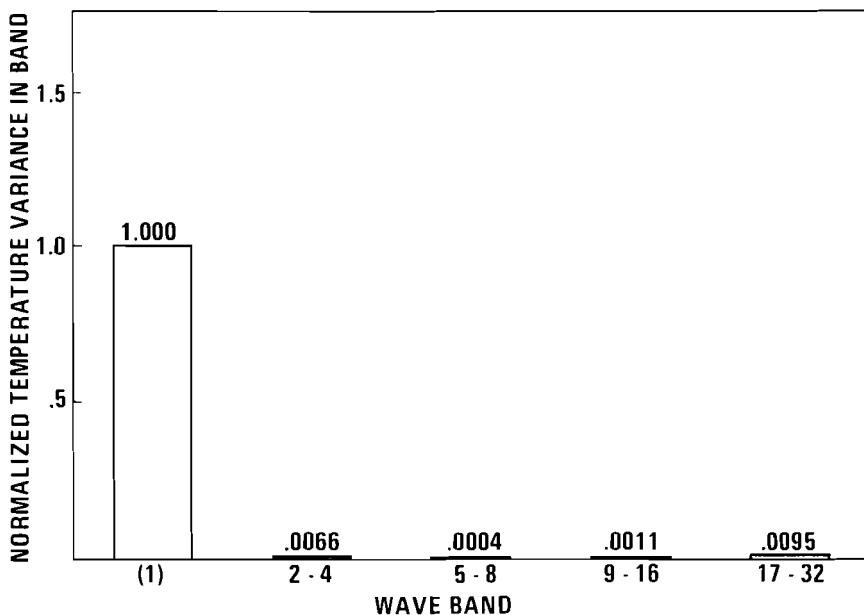


Fig. 4(c) Histogram showing temperature variance in each of five bands of consecutive wave numbers.

spectral gap approach advocated in Section I may prove superior to such classical parameterization approaches in representing such phenomena.

5 Concluding remarks

The results of this study suggest that using the full dynamic equations in spectral form to predict the interactions among large-scale atmospheric eddies and small-scale eddy ensembles, without having to represent intermediate-scale eddies, could be more realistic than using the usual parameterization approach. Specifically, the results of this simplified model of dry convective adjustment show:

- (i) in this model, there is a clear spectral gap in the nonlinear interactions affecting large-scale eddies.
- (ii) in this model, the nonlinear convective ensemble heat transport (i.e. the large-scale components of products of small-scale components of convective vertical velocity and small-scale components of temperature) apparently has significant *time* modulation, possibly due to ensemble energy propagation in a *space*-varying large-scale environment. The ensemble heat transport time variation appears independent of the time variations of the large-scale fields in the sense that the nonlinear transport apparently would vary significantly with time even if the large-scale fields were constant in time.

In view of (ii), the usual parameterization assumption that large-scale nonlinear transports are in a kind of quasi-equilibrium dictated by the large-scale fields (and possibly their recent histories) might not be accurate in general. In order to forecast these nonlinear transports, it may be necessary to specify initial values of both the large-scale fields and the large-scale nonlinear transport fields. If analogous convective ensemble time variation occurs in the atmosphere (as, for example, in east coast winter storms), the required large-scale initial distributions of nonlinear transport fields could, perhaps, be inferred from the intensity of small-scale oscillations (in space or time) recorded by observing stations.

Acknowledgments

During my recent service at McGill University, this research was supported by the National Research Council of Canada, under grant number 280-98, and by the Atmospheric Environment Service. More recently, it was supported by NAVAIR, under grant number NOO 173-76-C-0022. Computing support was provided by the National Center for Atmospheric Research. I am indebted to Drs Terry Williams, Steve Piacsek, Lothar Ruhnke, Jacques Derome, Harley Hurlburt, and Dana Thompson for valuable comments and assistance in the course of this research. I am especially indebted to Dr Tom Warn for valuable suggestions that gave the initial inspiration for this study. The fine technical assistance from Ms Karon Christensen and Ms Margaret Mikota in preparing this manuscript is greatly appreciated.

References

- ARAKAWA, A. and W.H. SCHUBERT. 1974. Interaction of cumulus ensemble with the large-scale environment, Part I. *J. Atmos. Sci.* **31**: 674-701.
- BATES, J.R. 1972. A generalization of CISK theory. *J. Atmos. Sci.* **30**: 1509-19.
- BRUNET, N. 1974. Time spectral analysis of space-averaged precipitation. Master's thesis, McGill University, 78 pp.
- CHARNEY, J.G. 1971. Geostrophic turbulence. *J. Atmos. Sci.* **28**: 1087-95.
- and A. ELIASSEN. 1964. On the growth of the hurricane depression. *J. Atmos. Sci.* **21**: 68-75.
- DEARDORFF, J.W.; G.E. WILLIS; and D.K. LILLY. 1969. Laboratory investigation of non-steady penetrative convection. *J. Fluid Mech.* **35**: 7-31.
- . 1974. Comments on the paper by A.K. Betts, "Non-precipitating cumulus convection and its parameterization." *Quart. J. Roy. Meteor. Soc.* **100**: 122-3.
- DIETRICH, D.E. 1975. Numerical solution of fully implicit energy conserving primitive equations. *J. Meteor. Soc. Japan* **53**: 222-5.
- ; B.E. MCDONALD; and A. WARN-VARNAS. 1975. Optimized block-implicit relaxation. *J. Comp. Phys.* **18**: 421-39.
- HÖGSTRÖM, A.S. and U. HÖGSTRÖM. 1975. Spectral gap in surface-layer measurements. *J. Atmos. Sci.* **32**: 340-50.
- LINDZEN, R.S. 1974. Wave-cisk in the tropics. *J. Atmos. Sci.* **31**: 156-79.
- MCINTYRE, M.E. 1968. The axisymmetric convective regime for a rigidly bounded rotating annulus. *J. Fluid Mech.* **32**: 625-55.
- NINOMIYA, K. 1975. Large-scale aspects of air-mass transformation over the East China Sea during AMTEX '74. *J. Meteor. Soc. Japan* **53**: 285-303.
- OGURA, Y. 1964. Frictionally controlled, thermally driven circulations in a circular

- vortex with application to tropical cyclones. *J. Atmos. Sci.* **21**: 610-21.
- OOYAMA, K. 1964. A dynamic model for the study of tropical cyclone development. *Geofis. Intern. (Mexico)* **4**: 187-98.
- WILLIAMS, G. 1969. Numerical integration of the three-dimensional Navier-Stokes equations for incompressible flow. *J. Fluid Mech.* **37**: 727-50.
- WILLIAMS, R.T. 1967. Atmospheric frontogenesis: a numerical experiment. *J. Atmos. Sci.* **24**: 627-41.
-

Experiments with a Polar Filter and a One-Dimensional Semi-Implicit Algorithm

Philip E. Merilees¹

University Corporation for Atmospheric Research²
Boulder, Colorado

and

Pierre Ducharme and Ghislain Jacques

McGill University
Montreal, Quebec

[Manuscript received 6 August 1976; in revised form 5 November 1976]

ABSTRACT

The numerical integration of the dynamical equations on a latitude-longitude grid requires excessively small time steps due to the convergence of meridians. Space filtering in the polar regions has generally been used to alleviate this restriction. Such filtering does not distinguish

between low and high frequencies so that it can lead to errors in the meteorological modes. An alternative solution may lie in the use of a semi-implicit technique in one dimension. These problems are explored with the aid of numerical models of the shallow-water equations on a sphere.

1 Introduction

The numerical integration of the equations governing atmospheric flow using a latitude-longitude grid presents certain practical problems. One of the problems is due to the convergence of the meridians near the north and south poles. This property requires that a very small time step be used to avoid computational instability. Of the various solutions that have been proposed or adopted, the procedure of Fourier filtering first suggested by Arakawa and tested by Holloway et al. (1973) has found considerable favour. It was used by Holloway et al. and by Merilees (1974) with apparently no noticeable detrimental effects. In retrospect, we might have expected to pay a price for a benefit that appeared to be almost free. This paper will report on some experiments originally designed to provide unambiguous answers to the question of the relative efficiency of the pseudospectral algorithm and the 4th-order finite difference schemes, but which turned out to be a study of polar filtering errors. This occurred because in the experiments performed, the polar filtering turned out to be a

¹Present Address: McGill University, Montreal, Quebec.

²The University Corporation for Atmospheric Research operates the National Center for Atmospheric Research, which is sponsored by the National Science Foundation.

source of error, making it very difficult to compare efficiencies of the two numerical schemes.

The numerical experiments performed are novel in the sense that the exact solution of the equations is known. This is accomplished by artificially forcing the equations by terms that imply an exact *specified* solution. Thus the numerical results are always compared to the exact solution. The resolution of the numerical models is large compared to the wavelength of the specified solution so that the resulting errors are relatively small. Nevertheless, these errors are bothersome because they appear to neutralize any possible gain from higher order approximations to derivatives.

As an alternative to polar filtering some experiments with a one-dimensional semi-implicit algorithm have been performed, and we present a report on these experiments as well.

2 The experimental approach

When experiments are performed to test different numerical schemes or approaches one usually begins testing with relatively simple situations. For example, one may test stationary solutions as did Merilees (1973), and Williamson and Browning (1973). This is very useful since one knows the exact solution of the equations. In the case of the nonlinear shallow-water equations, this is the only known solution of the equations. Lacking the knowledge of the solution of the equations one is forced to perform sensitivity experiments. That is, one may perform a control experiment with very high resolution in space or time and regard such an integration as the exact solution. Other experimental results are then compared with the standard. The approach taken here is somewhat different. A solution is specified and then the equations modified to fit this solution. The modification takes the form of a forcing function applied to the basic shallow-water equations on a sphere. Thus the experiments are concerned with simulating solutions of the equations,

$$\frac{\partial u}{\partial t} = -\frac{g}{a \cos \phi} \frac{\partial h}{\partial \lambda} - \frac{u}{a \cos \phi} \frac{\partial u}{\partial \lambda} - \frac{v}{a} \frac{\partial u}{\partial \phi} + f^* v + G_1(\lambda, \phi, t) \quad (1)$$

$$\frac{\partial v}{\partial t} = -\frac{g}{a} \frac{\partial h}{\partial \phi} - \frac{u}{a \cos \phi} \frac{\partial v}{\partial \lambda} - \frac{v}{a} \frac{\partial v}{\partial \phi} - f^* u + G_2(\lambda, \phi, t) \quad (2)$$

$$\frac{\partial h}{\partial t} = -\frac{1}{a \cos \phi} \left[\frac{\partial}{\partial \lambda} (hu) + \frac{\partial}{\partial \phi} (hv \cos \phi) \right] + G_3(\lambda, \phi, t) \quad (3)$$

where $f^* = 2\Omega \sin \phi + u \tan \phi/a$ and the other symbols have their usual meteorological meaning. The functions G_1 , G_2 , G_3 are specified functions such that the solution of (1) to (3) is given by

$$u = aK(m \cos^{m-1} \phi \sin^2 \phi - \cos^{m+1} \phi) \cos(m\lambda - \omega t) + a\Lambda \cos \phi \quad (4)$$

$$v = -maK \cos^{m-1} \phi \sin \phi \sin(m\lambda - \omega t) \quad (5)$$

$$h = \frac{2\Omega a^2}{g} K \cos^m \phi \sin^2 \phi \cos(m\lambda - \omega t) + \frac{\Omega \Lambda a^2}{g} \cos^2 \phi + h_0 \quad (6)$$

where m is the zonal wave number; K, Λ are arbitrary parameters and

$$\omega = \left[\frac{m(m+3)\Lambda - 2\Omega}{(m+1)(m+2)} \right] m. \quad (7)$$

We note that the solution is nondivergent for all time and is in a state of near geostrophy. The required expressions for G_1, G_2, G_3 may be obtained by substituting (4) to (6) into (1) to (3). In all of the experiments reported here, $m = 4$ while $K = \Lambda = 7.848 \times 10^{-6} \text{ s}^{-1}$ and $h_0 = 3000 \text{ m}$. The structure of the specified solution is shown in Fig. 1. With the given conditions the specified solution translates eastward at a speed of 12.2 degrees of longitude per day. In this map and any subsequent maps we present only one quarter of the entire field because of their symmetry properties. The "window" covers an interval of 180° of longitude, 90° of latitude. Both coordinates vary linearly.

The experiments proceeded as follows. Initial conditions obtained from the specified solution were applied to the numerical model, which was then integrated for a period of 8 days. The numerical solution obtained was then compared with the specified solution either in the form of difference maps or in an area-weighted RMS sense for each of the three variables.

The models used were formulated on a latitude-longitude grid with the same angular interval in both directions. The grid is displaced one-half of a grid length away from the poles. The 4th-order model and the pseudospectral model are as described in Merilees (1974) and are identical except for the evaluation of derivatives. One important point is that the polar filter operates so that wave numbers greater than 3 are filtered at the grid latitude circle closest to the poles; then wave numbers greater than 9 at the next closest; wave numbers greater than 15 at the next, and so on. Thus wave number 4 is filtered at the grid latitude closest to the poles. The results of the numerical experiments were looked at in two ways. Firstly, we have calculated the ratio of the area-weighted root mean square difference between the numerical solution and the specified solution to the square root of the variance of the analytical solution. That is, if $X(\lambda, \phi, t)$ represents the analytical solution of one of the variables and $X^*(\lambda, \phi, t)$ represents the corresponding numerical solution, we have calculated

$$E^2 = \overline{(X - X^*)^2}$$

and

$$V^2 = \overline{(X - \bar{X})^2}$$

where

$$\overline{(\quad)} \equiv \frac{1}{4\pi} \int_0^{2\pi} \int_{-\pi/2}^{\pi/2} (\quad) \cos \phi \, d\phi \, d\lambda$$

and then taken the ratio of E to V as a relative measure of error. This ratio expressed in per cent is what is meant by the error plotted in the graphs. All graphs presented show the relative errors in the v -field. The relative errors in the u and h fields are very similar to that of the v -field as long as we compare the differences with that part of the u and h fields that vary with time.

Secondly, we have studied the distributions of the differences between the

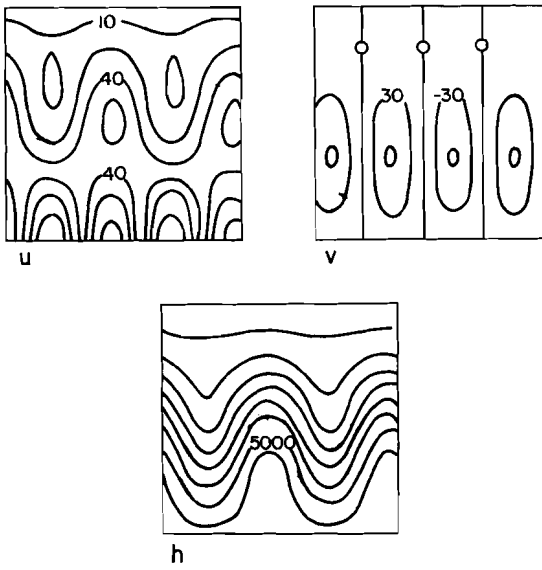


Fig. 1 The structure of the specified solution. Only one quarter of the global field is presented because of the symmetry. The equator is at the bottom of the “windows”; the pole at the top. The contour intervals are; u , 15 m s^{-1} ; v , 30 m s^{-1} ; h , 300 m .

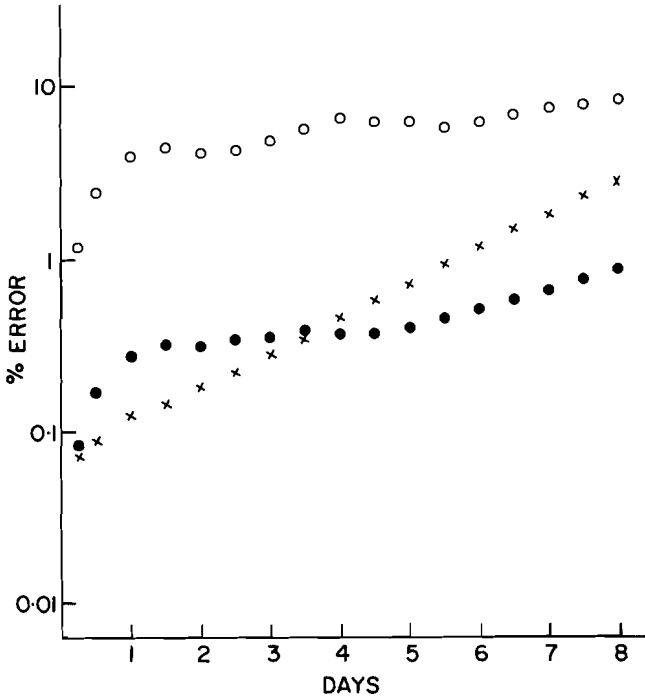


Fig. 2 The relative error in the v -field as a function of time obtained with different models employing a polar filter and a time step of 300 s . Open circles correspond to FD4-32, closed circles to FD4-64, and crosses to PS-32.

numerical solution and the specified solution and these results are presented in isopleth form.

A typical result and the one which led to this study of the polar filter is given in Fig. 2 showing the error in the v -component of the wind as a function of time for a 4th-order model with 64 grid points on a latitude circle (FD4-64), a 4th-order model with 32 grid points (FD4-32) and a pseudospectral model with 32 grid points (PS-32). Each of these were run with a time step of 5 min. We note that the error of the PS-32 is considerably less than that of the FD4-32. On the other hand the error of the PS-32 grows exponentially and exceeds that of the FD4-64 after four days of integration. Since the experiments were meant to test the hypothesis that the pseudospectral algorithm should be at least equivalent to a 4th-order scheme of twice the number of points, this result was of some concern. Further, the characteristics of the growth of error in the pseudospectral model were bothersome since the finite difference error grew very slowly after what appeared to be an initial adjustment period.

For these reasons various experiments with and without the polar filter were carried out.

3 Experiments with and without polar filter

In order to try to discover what was the cause of the exponential growth of error in the pseudospectral model, the first step was to integrate both the pseudospectral model and finite difference models without the polar filter. In Fig. 3 we present the results of such integrations where we have used a time step of 60 s. We note that the errors for the finite difference models remain almost the same while the errors in the pseudospectral model have decreased by two orders of magnitude. Further the growth rate of the errors in the pseudospectral model is considerably less. In fact the errors in the pseudospectral model appear to be almost entirely time truncation errors. This latter statement is supported by Fig. 4, which shows the errors in the pseudospectral model and the results of a theoretical calculation of the time truncation error. The theoretical curve is obtained from the solution of the time difference equation for a propagating wave whose frequency is equal to that of the specified solution. The time differencing is leap-frog, modified by the Robert filter (see Asselin, 1972).

The final link in the chain is provided by an experiment with a time step of 60 s, but using the polar filter (even though it is unnecessary). The error curves obtained are almost indistinguishable from the case with a time step of 300 s, and are thus not presented. The errors in the finite difference models appear to be due largely to space truncation error. This latter statement is supported by Fig. 5, which shows the error in the finite difference model at various times as a function of the number of grid points. Each of the cases was run without a polar filter and a time step of 60 s. The values plotted for a resolution of 64 were multiplied by 16, while those of resolution 128 were multiplied by 256 in accordance with an expected behaviour of space truncation errors of a 4th-order scheme. Except for the last two days of the integrations, the errors

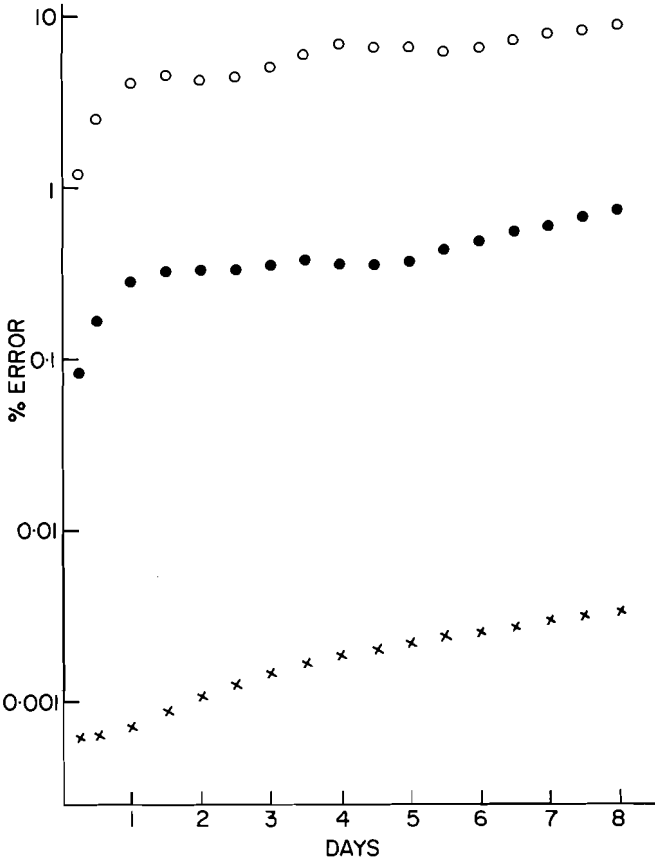


Fig. 3 Same as Fig. 2 except no polar filter and a time step of 60 s.

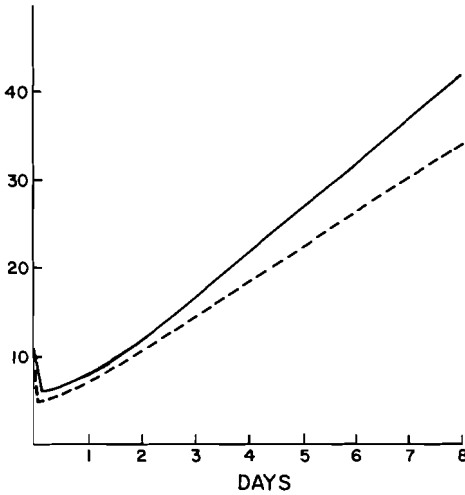


Fig. 4 Comparison between errors in the v -field for a PS-32 model with a time step of 60 s and no polar filter (dashed line) and the theoretical error associated with time discretization of a simple eastward propagating wave. The ordinate is such that 10 corresponds to a relative error of 0.001%.

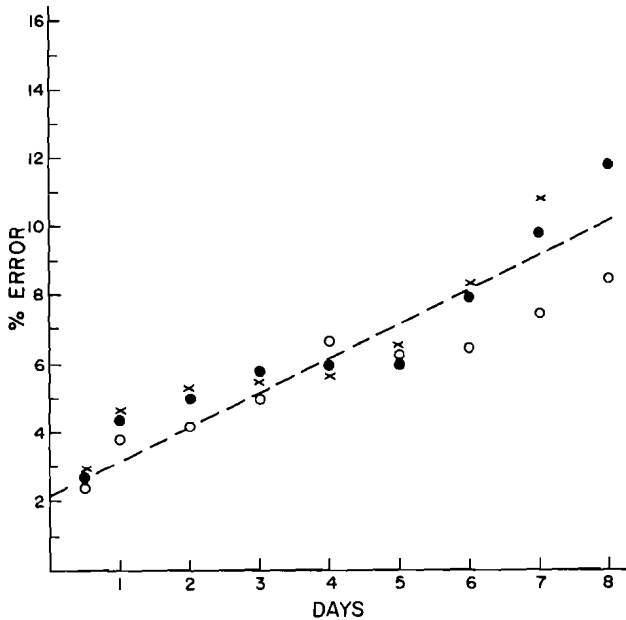


Fig. 5 The relative error in the v -field as a function of time obtained with different resolutions of the finite difference model with no polar filter and a time step of 60 s. Open circles correspond to FD4-32, closed circles to FD4-64, and crosses to FD-128. Values for FD4-64 were multiplied by 16 and for FD4-128 by 256.

seem to follow reasonably well what one would expect from space truncation errors.

One might expect the space truncation error to be so small in the case of the finite difference of resolution 128 that the error due to polar filtering would show up. This is not the case, however, because with a resolution of 128 points, the closest grid latitude (where wave number 4 is filtered) is considerably closer to the pole, and so the effect produced by filtering will be correspondingly less severe.

These results permit us to conclude that the application of the polar filter produces errors that grow rapidly and within a relatively short period of time may nullify any gain in accuracy obtained from the use of the pseudospectral algorithm. This latter statement is supported by the results of an experiment with the PS-32 model and a special polar filter. The special polar filter does not eliminate completely any wave number, but extrapolates the amplitudes from a specified latitude in accordance with the near-pole behaviour of Fourier amplitudes (Orszag, 1974). The results of that experiment showed a similar exponential growth rate as the experiment with the regular polar filter except that the absolute values were smaller.

4 The structure of the error due to polar filtering

Even though the use of polar filtering causes a growing error in the experiments

described here, the absolute value of these errors is not very large. Errors of the order of 1 to 10% translate into absolute values of 0.3 to 3 m s⁻¹ in the north-south component of the wind in a RMS sense, and these occur only after about eight days of simulation. Compared to other sources of error in prediction models, these magnitudes are certainly quite small. On the other hand, the model and initial conditions used are certainly quite simple compared to prediction and general circulation models that are in general use. Further, the fact that the error at least begins in the polar regions is bothersome because of the past history of difficulties in the long-term simulation of the atmosphere (Holloway et al., 1973). Thus it was deemed important to examine more closely the structure of the error due to polar filtering. During the eight-day integrations, the polar filtering does not have much effect on the errors of the finite differences models for reasons stated above. Thus we will examine the structure of the errors in the pseudospectral model produced by the polar filtering and compare it with the sorts of errors obtained when no polar filtering is applied.

In Fig. 6 we present the difference between the numerical solution and the specified solution after 1.5 days in the case of no polar smoothing, while Fig. 7 has polar smoothing applied. We note that the polar smoothing has generated errors of the order of 0.2 m s⁻¹ in the wind fields near the poles. This is basically due to the fact that the specified solutions have wind component values of this order in this region. The errors in the case of no polar smoothing are, as expected, of very small magnitude and have a structure very much the same as the varying time part of the specified solution. This basic structure persists for the entire eight-day period of integration as shown in Fig. 8.

The error field in this case is originally 90° out of phase with the specified solution. However, it very rapidly propagates to be about 180° out of phase and then maintains this relative phase by translating with the same phase speed as the specified solution. This behaviour indicates that the error is largely due to the smoothing effect of the Robert filter.

The error field in the case of the polar filter (Fig. 9) has a rather different behaviour. The phase relation to the specified solution is difficult to determine as the error field is strongly tilted with latitude. Since the specified solution has no tilt, the error is due to the tilt in the numerical solution. The tilting produces transports of momentum and we notice a deficit of momentum in latitudes around 60°N (and south) and an excess of momentum in the equatorial latitudes. We also note that the numerical solution has transported mass from lower latitudes to the higher latitudes.

5 An alternative to polar filtering

We have seen that the polar filtering produces errors which have the effect of changing the latitudinal distribution of mass and momentum under the conditions of these experiments. Such a tendency could be detrimental to the successful simulation of long-term distributions of atmospheric variables, even though the magnitude of the errors in these experiments is small. There is an alternative

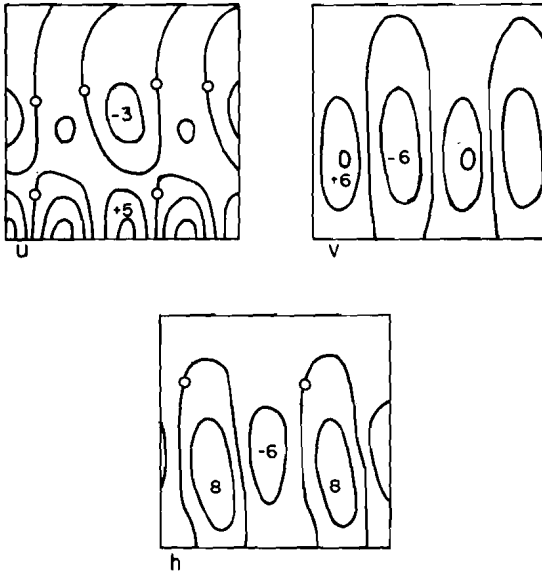


Fig. 6 The structure of the error fields after 1.5 days obtained with the PS-32 model, a time step of 60 s and no polar filter. Contour intervals: u , $2 \times 10^{-4} \text{ m s}^{-1}$; v , $3 \times 10^{-4} \text{ m s}^{-1}$; h , $4 \times 10^{-3} \text{ m}$. Geometry is the same as Fig. 1.

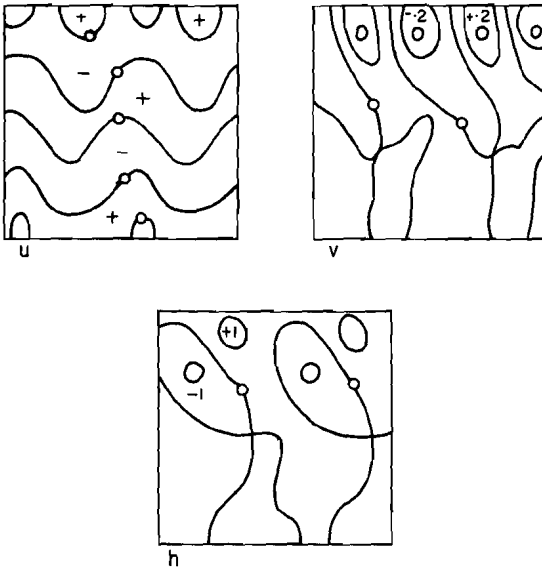


Fig. 7 Same as Fig. 6 except with the polar filter and contour intervals: u , 0.1 m s^{-1} ; v , 0.1 m s^{-1} ; h , 1 m .

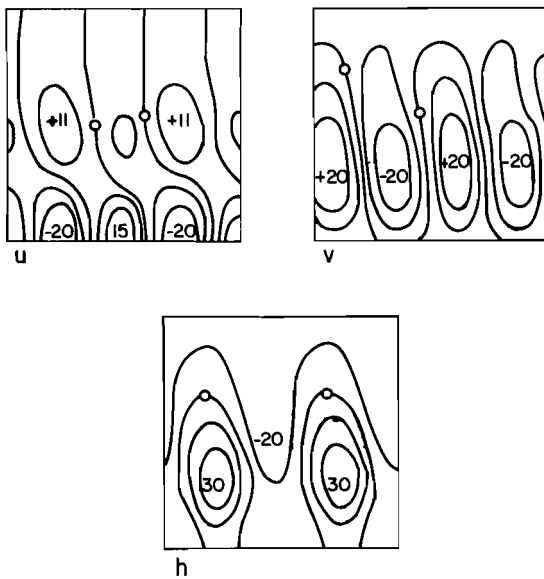


Fig. 8 Same as Fig. 6 except after eight days and contour intervals: u , $6 \times 10^{-4} \text{m s}^{-1}$; v , $6 \times 10^{-4} \text{m s}^{-1}$; h , $10 \times 10^{-3} \text{m}$.

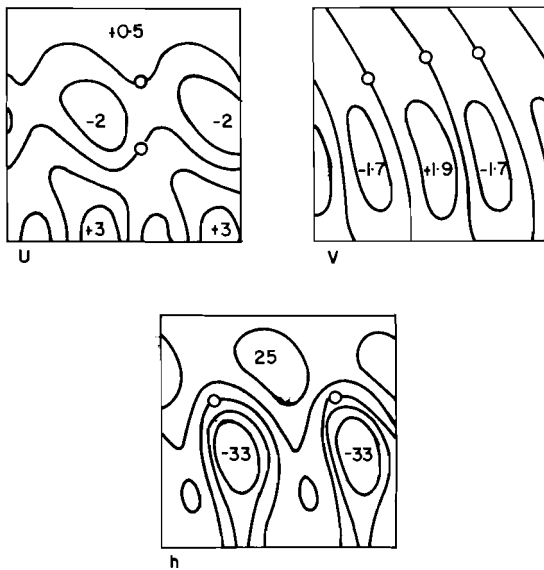


Fig. 9 Same as Fig. 7 except after eight days and contour intervals: u , 1 m s^{-1} ; v , 1 m s^{-1} ; h , 10 m .

to the polar filtering other than an explicitly stable time step, which makes use of a semi-implicit algorithm.

The semi-implicit algorithm was designed by Robert (1969) to operate in conjunction with a spectral model. Its application to the shallow-water equations over the sphere requires the solution of a Helmholtz equation. In terms of the spectral model such an application is relatively simple; in terms of a grid point model it is considerably more difficult. However, our interest in such an algorithm is simply to avoid the small time step necessary because of the convergence of meridians.

Thus we apply the algorithm in a one-dimensional sense along latitude circles, in which case we require the solution of a one-dimensional Helmholtz equation with periodic boundary conditions. Such a solution is easily accomplished with a fast Fourier transform (FFT).

We may write (1) to (3) without approximation as

$$\frac{\partial u}{\partial t} = - \frac{g}{a \cos \phi} \frac{\partial h}{\partial \lambda} + A \quad (8)$$

$$\frac{\partial v}{\partial t} = + B \quad (9)$$

$$\frac{\partial h}{\partial t} = - \frac{\bar{h}}{a \cos \phi} \frac{\partial u}{\partial \lambda} + C \quad (10)$$

where

$$\bar{h} = \frac{1}{2\pi} \int_0^{2\pi} h d\lambda$$

and is a function of latitude and time, and A , B , C represent all the remaining terms. We treat (9) explicitly and the terms A and C explicitly, so that the semi-implicit algorithm will take the form

$$u^{t+1} - u^{t-1} = - \frac{g\Delta t}{a \cos \phi} \frac{\partial}{\partial \lambda} (h^{t+1} + h^{t-1}) + 2\Delta t A^t \quad (11)$$

$$h^{t+1} - h^{t-1} = - \frac{h\Delta t}{a \cos \phi} \frac{\partial}{\partial \lambda} (u^{t+1} + u^{t-1}) + 2\Delta t C^t. \quad (12)$$

If we now express the fields, u , h , A , C in a finite Fourier series at the particular latitude, then (11), (12) will be transformed into a number of pairs of algebraic equations to be solved for the new amplitudes of the Fourier coefficients of u and h which can then be used to reconstruct the fields at the grid points. This procedure will be the same for both the pseudospectral algorithm and a finite difference model, except the finite difference model will introduce a response function multiplying the differentiated terms. Of course one can generalize the procedure to include many other terms simply by expressing each term as the sum of two terms, one of which is linear with respect to functions of longitude. In the experiments we have performed, we have only treated the pressure gradient and divergence terms in this way.

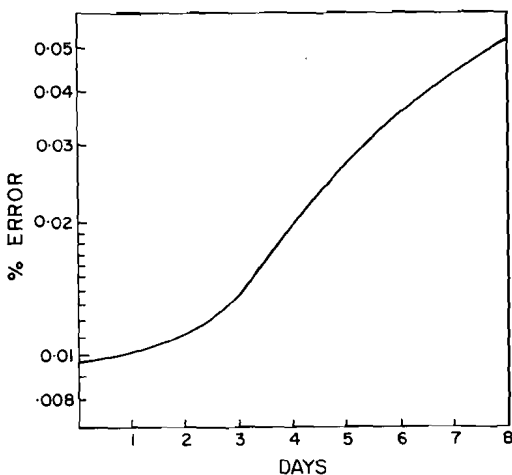


Fig. 10 A smoothed representation of the relative error in the v -field as a function of time obtained with the PS-32 model employing the one-dimensional semi-implicit algorithm and a time step of 600 s.

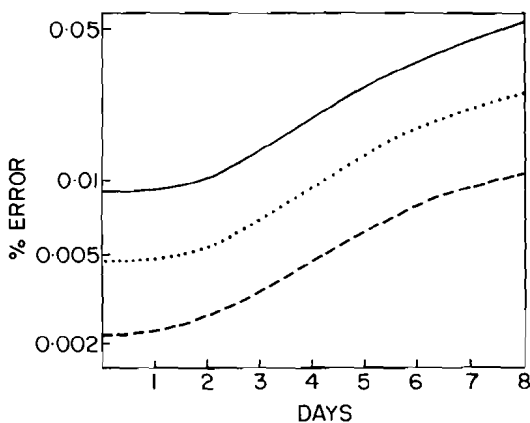


Fig. 11 Same as Fig. 10 except additional curves with time steps of 300 s (dotted) and 150 s (dashed).

The code for the pseudospectral model was modified to apply this algorithm and the polar filter was removed. Experiments of the same nature as previously described were then performed. It was found that the model with the semi-implicit algorithm was stable with time steps twice as large as that permitted with the polar filtering. This is consistent with the fact that the polar filter was applied only for latitudes greater than 60°N and 60°S . The results are shown in Fig. 10 for the v component of the wind. Note that the relative error remains less than 0.05% throughout the eight-day integration whereas the relative error using the polar filter reaches 1% by the sixth day. The error level at this point is about 10 times larger than that obtained with the explicit time differencing, but we have used a time step 10 times larger. The errors obtained with

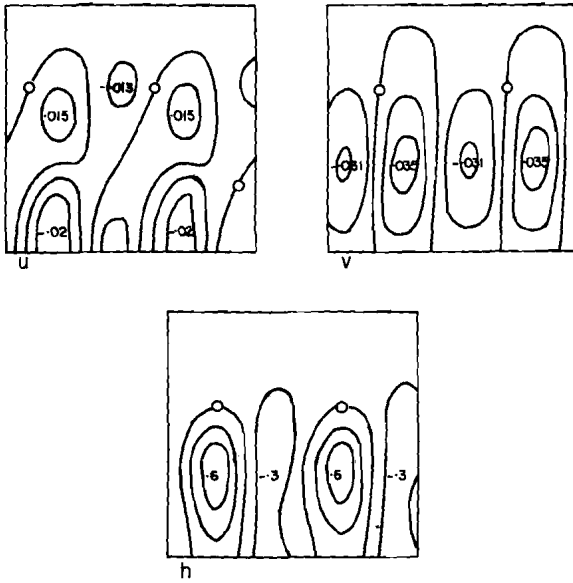


Fig. 12 The structure of the error fields after eight days with the PS-32 model employing the one-dimensional semi-implicit algorithm and a time step of 600 s. Contour intervals: u , 0.01 m s^{-1} ; v , 0.015 m s^{-1} ; h , 0.2 m. Geometry is the same as Fig. 1.

the one-dimensional semi-implicit algorithm vary approximately linearly with Δt , as shown in Fig. 11. They appear to be due to the use of the Robert filter which has a slight smoothing effect on the numerical solution. This idea was supported by experiments performed with a different value of the Robert filter coefficient, which showed that as it was increased the errors increased in a proportional way.

The structure of the error fields after eight days of integration are shown in Fig. 12. We note that the errors show no tendency to have a “tilt” nor do they indicate any accumulation of mass nor momentum in any latitude belts.

6 Conclusion

The use of polar filtering to increase the time step in a numerical model of the shallow-water equations has been shown to cause errors that work against the increased accuracy expected from higher order difference schemes. Further, the structure of the errors indicates that polar filtering can lead to artificial transports of mass and momentum. It is not clear if similar effects will be produced in realistic global circulation models, but it may be worthwhile to perform some control experiments without polar filtering.

The one-dimensional semi-implicit algorithm performed extremely well in the cases tested. Since the algorithm can be solved using a FFT, it can be efficiently implemented. In fact, as a replacement for a polar filter its implementation requires little additional computer time since the polar filter uses FFTs to accomplish its purpose.

The use of a semi-implicit scheme in order to increase the time step also makes sense from a physical point of view, because it modifies only the high-frequency motions whereas the polar filter modifies both the high frequencies and low frequencies.

Acknowledgments

A large portion of this work was carried out at the National Centre for Atmospheric Research and it is a pleasure to acknowledge the work of Ray Fabec who programmed many of the experiments and contributed in other significant ways. Further support was provided by the National Research Council of Canada and the Atmospheric Environment Service of Canada.

References

- ASSELIN, R. 1972. Frequency filter for time integrations. *Mon. Wea. Rev.* **100**: 487-90.
- HOLLOWAY, J. LEITH, JR; MICHAEL J. SPELMAN; and SYUKURO MANABE. 1973. Latitude-longitude grid suitable for numerical time integration of a global atmospheric model. *Mon. Wea. Rev.* **101**: 69-78.
- MERILEES, P.E. 1973. The pseudospectral approximation applied to the shallow-water equations on a sphere. *Atmosphere* **11**: 13-20.
- . 1974. Numerical experiments with the pseudospectral method in spherical coordinates. *Atmosphere* **12**: 77-96.
- ORSZAG, S.A. 1974. Fourier series on spheres. *Mon. Wea. Rev.* **102**: 56-75.
- ROBERT, A.J. 1969. Integration of a spectral model of the atmosphere by the implicit method. *Proc. WMO/JUGG Symp. Numerical Weather Prediction*, Tokyo, Japan, 26 Nov.-4 Dec. 1968: VII-19-VII-24. Tokyo: Japan Meteorological Agency, March 1969.
- WILLIAMSON, D.L. and G.L. BROWNING. 1973. Comparison of grids and difference approximations for numerical weather prediction over a sphere. *J. Appl. Meteor.* **12**: 264-74.
-

An Alberta Study to Objectively Measure Hailfall Intensity

G.S. Strong¹ and E.P. Lozowski

Division of Meteorology

Department of Geography, University of Alberta, Edmonton, Alberta

[Manuscript received 14 June 1976; in revised form 10 December 1976]

ABSTRACT

During the summer of 1973, two networks of hail detectors were established in a hail-prone region of southern Alberta, in conjunction with the hail suppression investigations being carried out by Alberta Hail Studies (ALHAS).² Two hundred and seventy-two farmer volunteers maintained the detectors in two regions totalling 1600 mi², providing a mean station spacing of 2.5 mi. Five dense networks with a detector spacing of

0.25 mi were also operated during August.

These detectors successfully recorded the hailfall on 17 severe thunderstorm days. The areal coverage of the hailfall was found to be less sporadic than was popularly believed, and the data revealed two different spatial scales of hailfall variation. A preliminary examination of the significance of these results for the design of precipitation (and particularly hail) measuring networks is undertaken.

1 Introduction

Hail detectors, consisting of one-foot square pads of one-inch thick styrofoam wrapped in household aluminum foil, were independently developed and used with some success by Schleusener and Jennings (1960), and by Decker and Calvin (1961). Such "hailpads" have since been used successfully in Illinois (Changnon, 1969; Changnon and Towery, 1972) and in the midwest states (Hagen and Butchbaker, 1967; Butchbaker, 1968; Morgan and Towery, 1974).

A preliminary study was made to determine the feasibility of using hailpads in Alberta, both to discriminate where hail did or did not fall and also to obtain quantitative hailfall measurements. It was hoped that such data could be related to crop damage by hail, and aid in the evaluation of hail suppression efforts.

The theory, laboratory calibration, hailpad analysis techniques, network design, and results of this 1973 study were detailed by Strong (1974). Field verifications of the hailpad calibration have subsequently been presented by

¹Current affiliation: Alberta Hail Project, Mynarski Park, Alberta.

²The name was changed in 1974 to the Alberta Hail Project which is under the auspices of the Alberta Weather Modification Board, Three Hills, Alberta.

Lozowski and Strong (1975). The purpose of this paper is to review briefly the theory and operation of hailpads, to explain some important aspects of the 1973 measurements, and to relate these results to other field measurements of hailfall and to the design of future networks.

Theory

By solving the equation of motion for an idealized spherical hailstone in free-fall equilibrium, the terminal velocity w_T , is found to be a function of the diameter D_H :

$$w_T = \left(\frac{4\rho g}{3\rho_a C_D} D_H \right)^{\frac{1}{2}} \quad (1)$$

The following parameters were found to be most appropriate for typical Alberta conditions: drag coefficient $C_D = 0.6$, hailstone density $\rho = 0.89 \text{ g cm}^{-3}$, surface air density $\rho_a = 1.07 \times 10^{-3} \text{ g cm}^{-3}$, $g = 981.3 \text{ cm s}^{-2}$. Using these values, (1) becomes:

$$w_T = 13.5 D_H^{\frac{1}{2}} \quad (2)$$

where w_T is in metres/second and D_H in centimetres. This type of relation has been confirmed by Lozowski and Beattie (1975), who used high-speed photography to measure the terminal velocity of hailstones up to 1 cm in diameter during several 1974 Alberta hailstorms. They found that the curve $w_T = 13.3 D_H^{\frac{1}{2}}$ was a reasonable fit to their measurements. The kinetic energy of impact for such a hailstone is

$$e_I = \left(\frac{\pi \rho^2 g}{9 \rho_a C_D} \right) D_H^4 \quad (3)$$

or $4.23 \times 10^{-2} D_H^4$ Joules for the same Alberta conditions, where D_H is in centimetres.

The Hailpad Concept and Calibration

A hailstone hitting a hailpad leaves a dent in the styrofoam-aluminum foil combination of a volume proportional to the kinetic energy absorbed by the hailpad (Lozowski and Strong, 1975). As a consequence of this result, a relation between hailstone diameter and dent diameter can be derived, for example, by dropping steel spheres onto hailpads. These must fall from an appropriate height to simulate the impact energy of spherical hailstones of the same diameter. The use of real ice spheres for calibration is virtually precluded by the requirement for drop heights of more than 50 m if the larger ice spheres are to approach their terminal velocity.

For the types of styrofoam and aluminum foil used in this work,³ the relation between dent diameter (D_D) and hailstone diameter (D_H) was found to be

$$D_H = 0.15 + 1.11D_D - 0.09D_D^2 \quad (4)$$

for $0.5 \text{ cm} \leq D_H \leq 5.5 \text{ cm}$.

³DOW Chemical Styrofoam type *FR and Reynolds Wrap heavy-duty aluminum foil (0.0010 in thickness).

In using (4) to relate dent diameters to hailstone diameters, and thereby to calculate hailfall energies from the recorded hailpad dents, several other implicit assumptions are made. These are that: hailstones are hard and do not shatter upon impact; hailstones which impact a second time after bouncing provide a negligible contribution to the total impact energy derived from the hailpad; hail dents are readily distinguishable from dents made by other objects such as raindrops, bird pecks, etc.

Measurement Uncertainties

Hailpads can be used to estimate hailstone size, and hence to infer mass, terminal velocity, impact momentum, and impact energy. It was estimated (Strong, 1974) that the maximum combined absolute error in the measured impact energy of a single hailstone due to the assumptions about hail density, sphericity, drag coefficient, air density, and to uncertainties in calibration and measurement, was $\pm 65\%$. Although this is an extreme value for an individual hailstone, and the actual error in the hailpad total will be smaller most of the time, it could be quite acceptable when dealing with energies ranging over four or five orders of magnitude. It should also be pointed out that the relative error in the comparison of two hailpads similarly exposed can be shown (Strong, 1974) to be considerably less than this.

One other source of error must be mentioned – that of estimating hailstone sizes from dents made by wind-blown hailstones. Here, the total impact energy is

$$e_{IT} = e_I + e_H = \frac{1}{2}m(w_T^2 + w_H^2) \quad (5)$$

where w_H is the wind speed. In this case the hailpad dent is elongated to an elliptical shape. For such dents, only the minor axis diameter (D_m) was measured, and this was assumed to be equal to the diameter (D_D) of the circular dent which would have been made by the same hailstone falling vertically. This assumption is reasonable since the horizontal partition of the energy is expected to contribute largely to elongating the dent and not to increasing its depth. Thus, the measure of impact energy obtained from the hailpad is approximately the vertical partition (e_I) of the energy alone, and it does not include the horizontal partition (e_H) of the energy, which can be quite large.

Hailpad Networks

Fig. 1 shows the two main hailpad networks of 1973. The Southern Network was within the ALHAS area of total cloud seeding, while only a few single storm seeding experiments were conducted over the Northern Network. In all, 272 hailpad stations were maintained, with an average station density of 1 per 6 mi² (15.5 km²), or a mean linear spacing of 2.5 mi (4.0 km). Five meso-meteorological stations recorded additional data on winds, rain, temperature, and humidity. Previous analysis of volunteered hail reports from local farmers suggested that typical hailswaths in Alberta were 2–5 mi (3–8 km) wide (Summers and Wojtiw, 1971). Consequently, in order to test the representativeness of measuring point hailfalls every 2.5 mi, five dense networks were operated

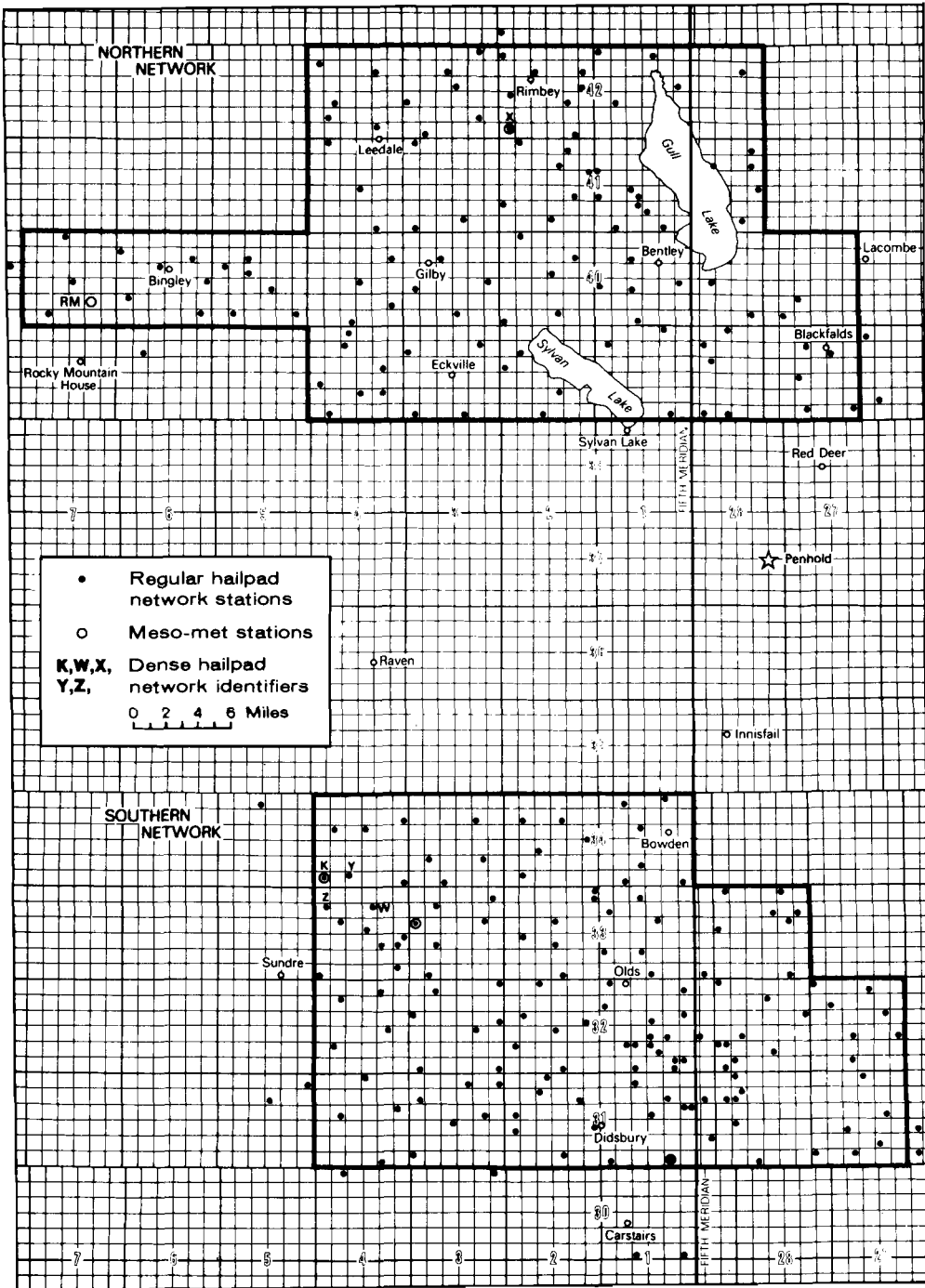


Fig. 1 The 1973 Alberta hailpad networks.

during August, each covering an area of either 1 mi² or 0.25 mi², and having hailpad spacings of 0.25 mi (one hailpad per 0.1 km²). The locations of the meso-meteorological stations and dense networks are indicated in Fig. 1.

Farmer volunteers carried out most of the daily maintenance of hailpad sites. Lack of time and money precluded the use of special hailpad stands, although the calibration had been made with a firm underlying surface. Instead, the hailpads were nailed to the ground with two 6 in spikes inserted through opposite corners. Subsequent field tests showed that this resulted in an under-estimate of impact energy ranging from 5 to 25%, depending on the softness of the surface underlying the hailpad.

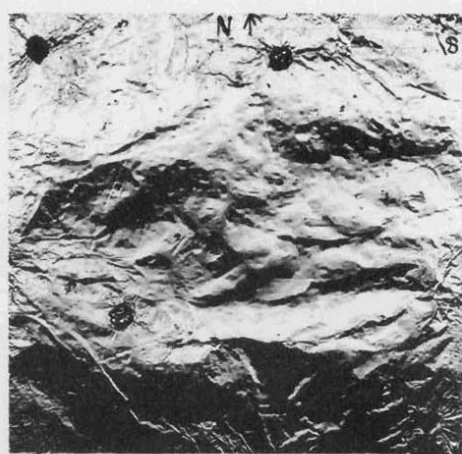
2 Principal results

Seventeen hailstorms struck the two main networks during the period 25 June to 27 August inclusive. A total of 763 hail-dented pads were collected for the study, yielding point values of impact energy ranging from 10⁻¹ to 2 × 10³ J m⁻². Fig. 2 depicts four of these hailpads with brief summaries of the derived data in the captions. The two holes in opposite corners of each pad were made by the spikes during installation. The wind estimates were made from the angles of dent streaks on the hailpad edges, although such estimates will not be discussed here.

One of the reasons for making hailpad measurements is to try to find relations between hailfall and crop damage that could be applied to the evaluation of the possible benefit of hail suppression efforts. Confidential hail insurance statistics for point locations were not readily available. Instead, less accurate crop damage estimates were obtained from hail report cards submitted by hailpad operators. Such estimates may unfortunately be biased and they may not be strictly comparable because they do not allow for differences in the time in the growing season, soil types, farming methods, local meteorological variations, damage caused by rain water run-off, and so on. In addition, it was not known whether the farmer estimated damage at the hailpad site or at another location on his farm where the hailfall may have been different. The major crop types at hailpad sites were barley, oats, and rape, the latter being the most susceptible to hail damage.

In spite of such uncertainties in crop damage estimates, we attempted to see whether a relation between hailfall impact energy and crop damage could be determined (Fig. 3). The implication of this scatter diagram is that relatively little damage (<20%) seems to occur unless the impact energy exceeds a lower critical value of about 50 J m⁻². Beyond an upper critical energy of about 450 J m⁻², the damage was always 100%. In between, a considerable scatter exists which can be reduced by more careful measurements of crop damage and the factors related to it. In Fig. 3, we have somewhat arbitrarily postulated a logarithmic dependence of crop damage upon impact energy as given by the straight line.

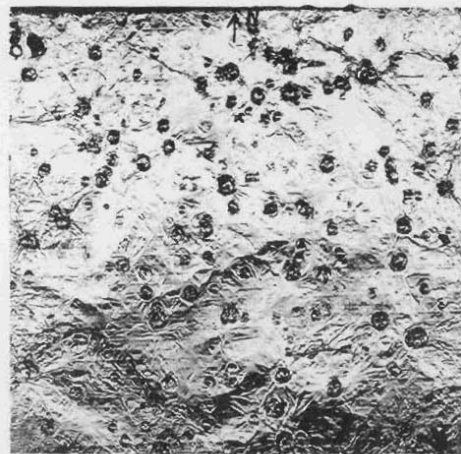
Thus, although impact energies can range over four or five orders of magnitude, the most important part of this range lies between about 50 and 450 J m⁻²,



Hailpad 2651, site G76; 16/Aug/73.

$D_H(\text{max}) = 2.0 \text{ cm}$; $M_H = 160 \text{ g m}^{-2}$;

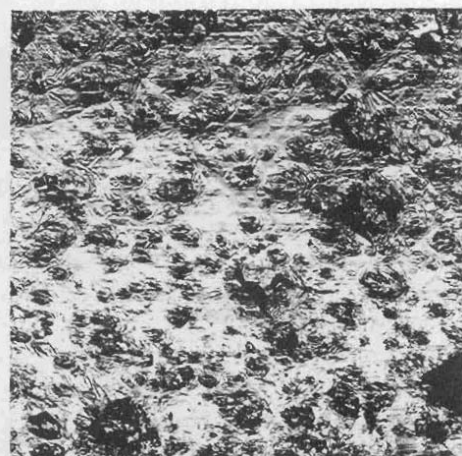
$E_I = 21 \text{ J m}^{-2}$; wind SW/light.



Hailpad 1656, site G1; 16/Aug/73.

$D_H(\text{max}) = 2.0 \text{ cm}$; $M_H = 1458 \text{ g m}^{-2}$;

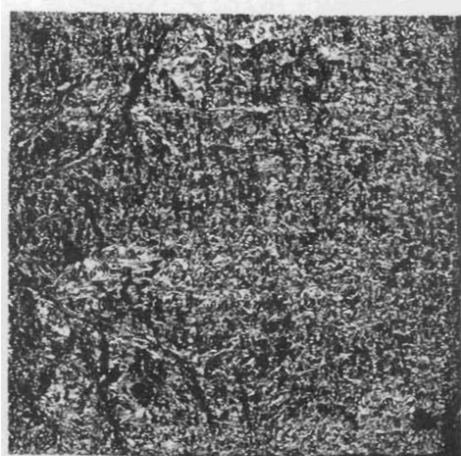
$E_I = 164 \text{ J m}^{-2}$; wind calm.



Hailpad 2621, D.N. X10; 16/Aug/73.

$D_H(\text{max}) = 3.8 \text{ cm}$; $M_H = 5256 \text{ g m}^{-2}$;

$E_I = 993 \text{ J m}^{-2}$; wind W/56 mph.



Hailpad 2003, site Q4; 24/Aug/73.

$D_H(\text{max}) = 1.3 \text{ cm}$; $M_H = 2860 \text{ g m}^{-2}$;

$E_I = 182 \text{ J m}^{-2}$; wind NNE/light.

Fig. 2 Four 1973 hail-dented hailpads with measured values of maximum hail size, hail mass, impact energy, and winds.

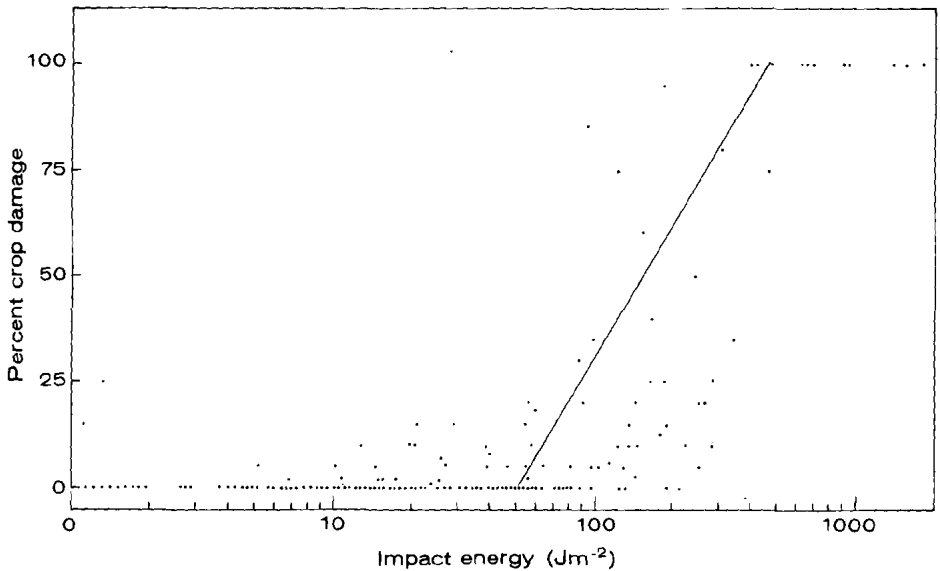


Fig. 3 Impact energy vs per cent crop damage (based on farmers' estimates). The dots are individual measurements. The line is a logarithmic relation joining the lower critical energy (50 J m^{-2}) and the upper critical energy (450 J m^{-2}).

since these values determine whether a farmer suffers a small or total crop loss. Fortunately, this is also the range of greatest accuracy for the hailpad, since it lies above the energy range where a very few dents may not be a representative sample, and below the regime where multiple dents and styrofoam breakage lead to additional uncertainty.

Another scatter graph was prepared for the total impact energy by adding to the abscissa values, the horizontal partition of impact energy due to the wind (obtained from farmers' estimates). This yielded an upper critical energy of around 800 J m^{-2} , a result similar to that obtained by Hagen and Butchbaker (1967). The relations between crop damage and other hailfall parameters such as impact momentum or hail mass were also examined, with a similar degree of scatter being found in each case.

Distributions of Energy Values in Alberta, North Dakota, and Illinois

As a comparison with other hailpad studies, Table 1 shows the distributions of impact energies for the 1973 Alberta network, for North Dakota (Hagen and Butchbaker, 1967) and for Illinois (Changnon and Towery, 1972). The unusual energy ranges result from the conversion of the units ft-lb ft^{-2} which were used in the U.S. studies. The energy-damage relation of Fig. 3 applied to Table 1 suggests that about 68% of the hailfall recorded within the Alberta hailpad networks during 1973 caused nil or light crop damage (less than 50 J m^{-2}). About 27% caused moderate to severe damage (50 to 450 J m^{-2}), while about 5% resulted in complete crop loss (greater than 450 J m^{-2}).

A greater proportion of light hailfalls were recorded in Alberta with 87%

TABLE 1. Comparison of hail intensity distributions in Central Alberta, North Dakota (Hagen and Butchbaker, 1967), and Illinois (Changnon and Towery, 1972)

Range of Impact Energy (J m ⁻²)	Per cent of Total Number of Hailpads		
	Central Alta (a) 1973	No. Dakota (b) 1966	Illinois (c) 1971-72
0.1- 50	67.5	—	—
50.1- 100	13.8	—	—
100.1- 146	6.0	—	—
0.1- 146	87.3	83.0	75.2
146.1- 292	5.4	8.7	9.2
292.1- 450	2.0	3.7	} 11.3
450.1-1000	4.4	4.0	
> 1000	0.9	0.6	4.3
No. of hailpads in study	763	319	913

being $\leq 146 \text{ J m}^{-2}$ (10 ft-lb ft⁻²), compared with 83% in North Dakota and 75% in Illinois. The higher figure for Alberta may be a real climatological difference, or it may mean that a more sensitive combination of styrofoam and aluminum foil was used. The minimum value in the North Dakota data was 5 J m^{-2} compared with 0.1 J m^{-2} for both the Illinois and Alberta data.

3 Impact energy analysis of hailswaths

The maps of impact energy for the 17 recorded hailstorms were subjectively contoured with isopleths of 0, 25, 50, 100, 200, 400, and 800 J m^{-2} . The contour increments were multiplicative because the energy gradient tends to increase along with the energy. Near the centre of the hailswaths or where the energy exceeded 800 J m^{-2} , the gradients were usually too high for adequate resolution with an average hailpad spacing of 2.5 mi (4 km). Subjective contour smoothing was minimal, and never at the expense of violating a station value of impact energy. A feature of these energy maps is the spatial continuity of the contours, especially the zero contour. This result tends to contradict a popular notion that hailfall patterns are very sporadic by nature. At least, if hailfall patchiness in these storms did occur, it must have been on a scale smaller than that resolvable by the present network. Only the hailstorms of 16 August and 23 August will be discussed here, since additional data from the dense networks were available for these days.

16 August 1973

This storm affected only the northern hailpad network, and it is depicted in Fig. 4. Recalling that energies exceeding 450 J m^{-2} usually cause 100% crop damage, this storm stands out as a major one. In addition to causing crop damage, the hail also smashed windows and vehicle windshields, killed small farm animals, and even pierced holes in barn roofs. It consisted of two main hailswaths, with the most severe one (according to other sources) all but missing the hailpad network. The southern swath (and second one in time) has two maxima, about 15 mi (24 km) apart. For the 17 hailstorms studied, this

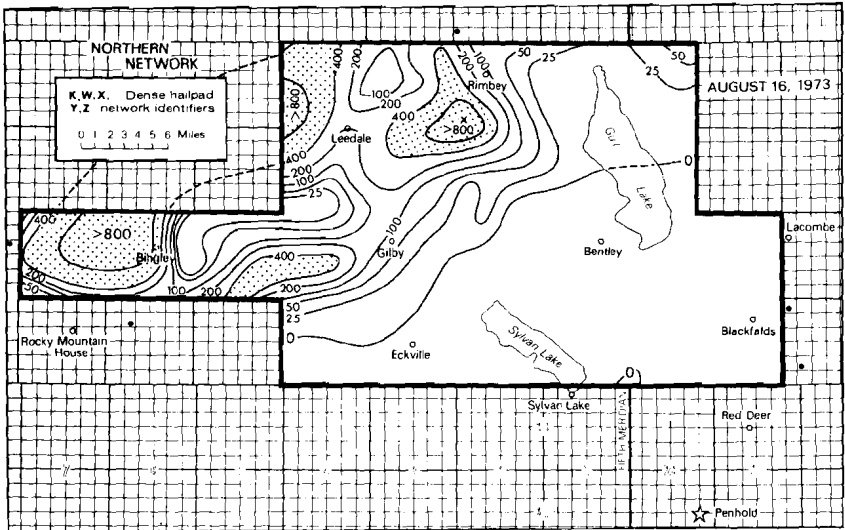


Fig. 4 Pattern of impact energy ($J m^{-2}$) over the Northern Network on 16 August 1973.

distance between maxima along a single swath varied from 10 to 15 mi (16 to 24 km), with an average of 12 mi (19 km). We shall refer to it as the wavelength of longitudinal variation.

Noting that dense network "X" (DNX) appears to have experienced impact energies exceeding $800 J m^{-2}$, we now turn to this smaller scale of 25 hailpads on one square mile plus two main network hailpads. Fig. 5 portrays both the individual values (upper right of site symbol) and the contours of impact energy, as well as the number of golfball or larger size hailstones per hailpad (in parenthesis below the symbol). Hail sizes in Alberta are reported in terms of familiar objects, viz.: shot, less than 0.6 cm diameter; pea, 0.6 to 1.2 cm; grape, 1.2 to 2.0 cm; walnut, 2.0 to 3.2 cm; golfball, 3.2 to 5.2 cm; larger than golfball, greater than 5.2 cm (Strong, 1974). With 12 of the 27 values of energy being less than $800 J m^{-2}$, a different scale of hailfall is immediately evident. The wavelength or distance between maxima on the fine scale appears to be about 1 mi (1.6 km), in contrast to the 10 to 15 mi (16 to 24 km) resolved by the larger scale network.

The original intention in setting up the dense networks was to test the representativeness of a single hailpad ($1 ft^2$ or $0.09 m^2$) as a measure of the hailfall over a larger area ($6 mi^2$ on the average for the 1973 network). In view of this, it is reasonable to ask whether the pattern of Fig. 5 may be due to a few scarce, large hailstones randomly hitting some hailpads but not others. If this were an important effect, it would cast doubt on the representativeness and hence the usefulness of the hailpad. The distribution of golfball and larger hailstones, whose contribution to the total impact energy ranges as high as 49% (at the two bottom right sites), might appear to suggest that the small-scale pattern is indeed a stochastic effect. Consequently, in order to investigate this

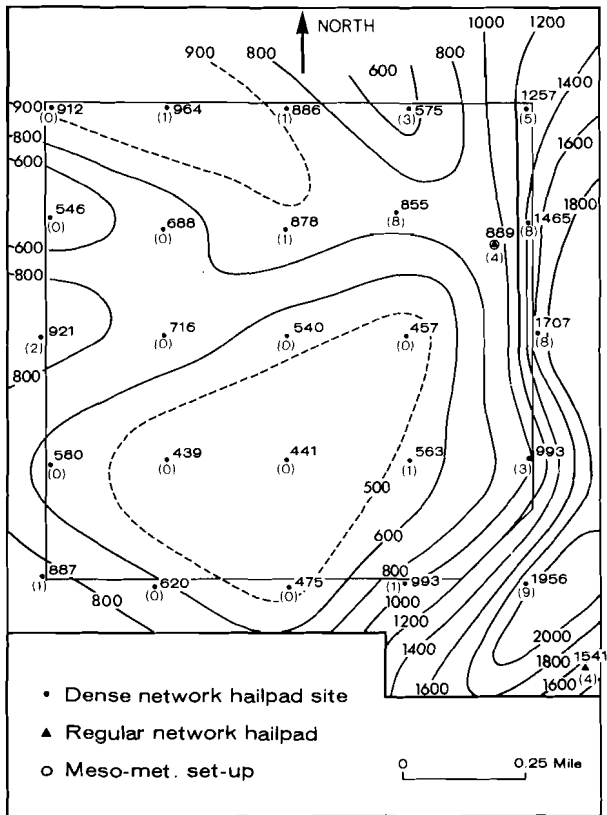


Fig. 5 Pattern of impact energy (J m^{-2}) for all hail sizes over the Northern Dense Network, DNX, on 16 August 1973. Values in parenthesis are the numbers of golfball and larger size hailstones per hailpad.

problem further, the energy pattern for various ranges of the hailstone size spectrum was examined.

Fig. 6 displays the energy pattern over DNX, excluding golfball and larger sizes, while Fig. 7 is the pattern without walnut or larger hailstones. In addition the patterns of both impact energy and hail mass over DNX on 16 August were inspected for all size ranges, including shot and pea sizes alone, grape size, and so on. These figures are not shown, but throughout this size spectrum the hailfall patterns were basically the same as those in Figs 5–7, with a minimum near the centre and maxima near the southeast, southwest, and northwest corners of the network. Inspection of the topographical features of DNX and of the winds during the storm show that exposure problems could not have been responsible for the pattern of Fig. 5 (Strong, 1974). It is reasonably certain then, that this pattern occurred throughout the hail size spectrum and is a result of the fine-scale structure of the hailstorm itself.

Concerning the question of hailpad representativeness, we note that indivi-

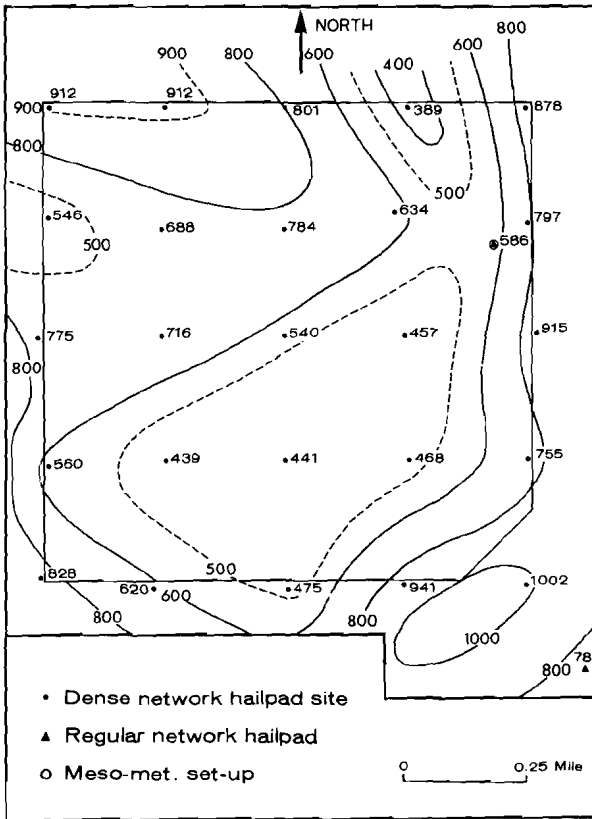


Fig. 6 Pattern of impact energy ($J m^{-2}$) over DNX on 16 August 1973 excluding the contribution to energy by sizes golfball, or larger.

dual measurements of energy density over this one square mile varied by more than a factor of two from the mean ($879 J m^{-2}$). This suggests that the error in estimating the average energy density over a section of land with a single hailpad measurement can exceed 100% due to such fine-scale variations. Nevertheless, as we shall see in section 4, a network of one pad per square mile may provide quite accurate estimates of the average energy density for the entire swath.

23 August 1973

The evening hailstorm of 23 August took a northward track, its major activity occurring to the west of both hailpad networks. However, it was of sufficient size and intensity to provide some hailpad data from both main networks and all five dense networks (Figs 8–11). August 23 showed the most sporadic patterns of the 17 storms studied, but it is discussed here because of the wealth of data gathered, including some mobile hailpad samples obtained while pursuing the storm in a truck.

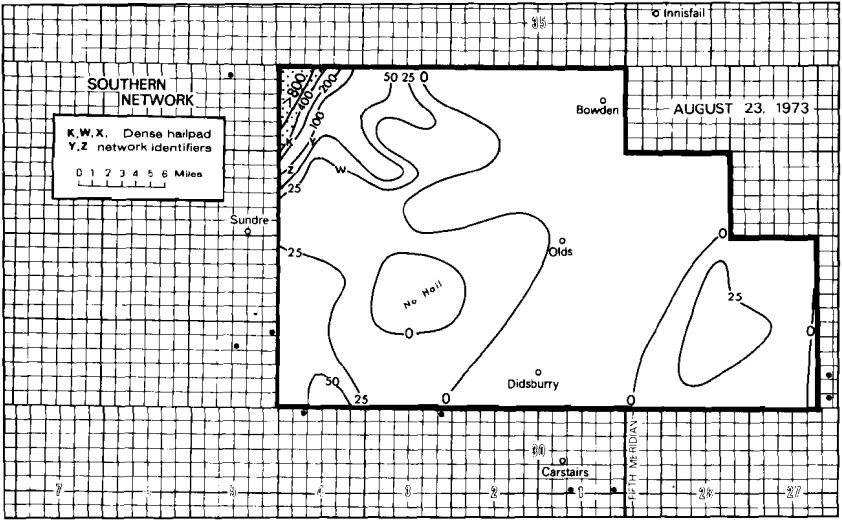


Fig. 8 Pattern of impact energy ($J m^{-2}$) over the Southern Network on 23 August 1973.

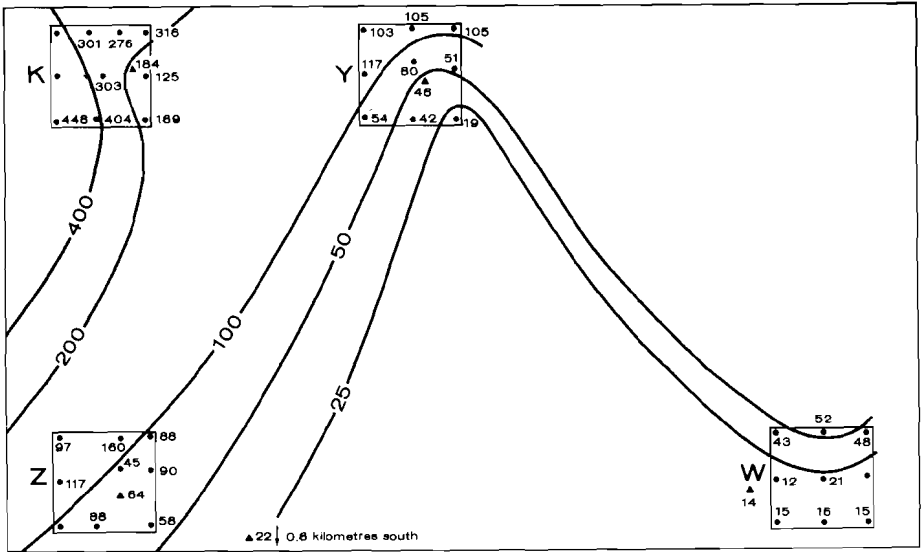


Fig. 9 Pattern of impact energy ($J m^{-2}$) over the Southern Dense Networks on 23 August 1973. The triangles are regular network stations and the dots are dense network stations. The length of the side of each square is 0.5 mi.

11), the pattern is opposite to that of 16 August, with a maximum where there previously had been a minimum, while the winds were from the same direction in both cases. This result supports the contention that these are real effects and are not due to exposure or other geographically determined factors. The main energy maximum is somewhat southwest of DNX ($>200 J m^{-2}$) as the main network map suggests, but there is also a secondary peak ($>175 J m^{-2}$)

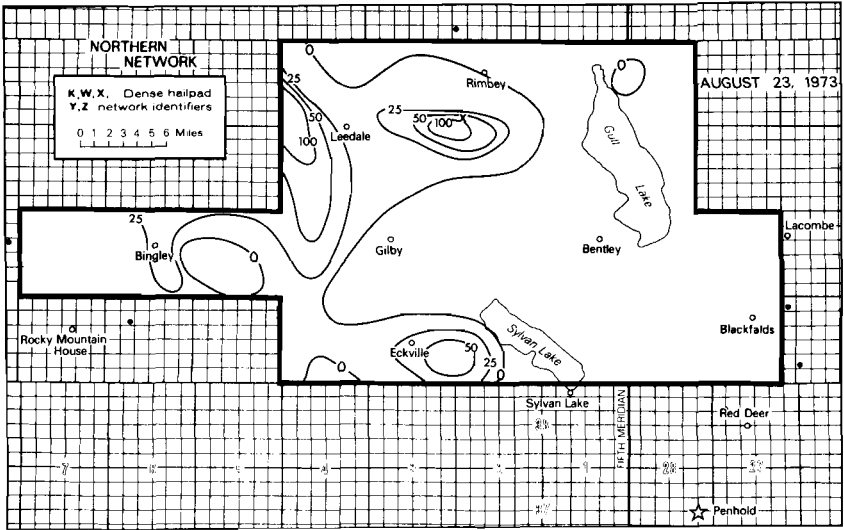


Fig. 10 Pattern of impact energy ($J m^{-2}$) over the Northern Network on 23 August 1973.

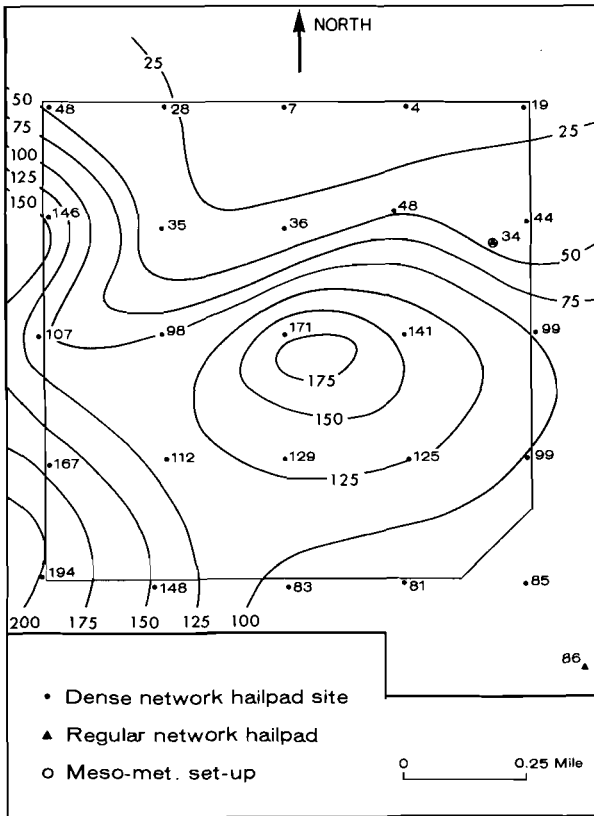


Fig. 11 Pattern of impact energy ($J m^{-2}$) over the Northern Dense Network, DNX, on 23 August 1973.

in the centre of the land section. Again, the “wavelength” on this fine scale appears to be about 1 mi.

4 Discussion

Hailpad Dimensions and Network Design

Although the 1973 networks were too small (24 mi wide by 36–55 mi long) to yield reliable data on hailswath lengths, the width of many of the swaths could be measured, as well as the longitudinal “wavelengths” of variations along a swath. For the particular storms considered, the width varied between 5 and 20 mi (8 and 32 km) with a mean of 10 mi (16 km), and the “wavelength” from 10 to 15 mi (16 to 24 km) with a mean of 12 mi (19 km). These results have important implications for the design of future hail detection networks in Alberta. Clearly, the average station spacing should be at most half the dominant scale of variation, i.e. 5 or 6 mi (8 or 10 km), simply in order to resolve the general hailfall pattern and to prevent aliasing.

Damaging hail (with an energy exceeding 50 J m^{-2}) occurred within paths 3 mi wide on the average (for example, see Fig. 4 for 16 August). This in turn suggests that a hailpad spacing of less than 3 mi (5 km) is required to adequately resolve the damaging hail. Furthermore, the dense networks show that a spacing of at most 0.5 mi (0.8 km) would be required in order to distinguish certain fine-scale patterns.

The effect of using hailpad spacings greater than 2.5 mi in 1973 was tested by systematically reducing the density of the data obtained from the storms discussed above by deleting some of the observations. This process revealed that the main large-scale patterns survived with 4-mi mean spacings, but that the patterns became unresolvable with mean spacings of 8 mi (13 km). There is another undesirable effect of changing the station density or of comparing data from networks of different densities. It was shown by deleting some of the hailpad observations that the mean values and the standard deviations of hailfall energy for a storm both change significantly when the network density is reduced. This problem will be considered in more detail in part 5.

Causes of the Observed Hailfall Patterns

No definitive explanation can be offered here for the two scales of hailfall variation noted; that is, wavelengths of about twelve miles, and of about one mile. Still smaller scale variations probably do exist, but these are the principal ones that have been detected with the present networks.

The formation of new convective cells on the right flank of existing thunderstorms which then propagate in a direction to the right of the cell motion (Newton and Katz, 1958; Browning, 1964; Renick, 1971; Chisholm and English, 1973), provides a possible explanation for the large-scale pattern. Fig. 4, for example, shows an energy maximum east-northeast of the town of Rocky Mountain House, and the energy appears to taper off to the east. At this point, perhaps a new cell started to hail, continued northeastward and then gave rise

to the next energy maximum near DNX. Such an explanation is consistent with the concept of a "hailstreak" within the larger "hailswath," as defined by Changnon (1970).

The small-scale maxima of the dense networks probably result from the turbulent nature of such storms, each cell having more than one region of hail concentration. Morgan and Towery (1974, 1975) observed the same scale of hailfall variation occurring within a similar dense hailpad network in Nebraska in 1973. Changnon and Barron (1971) noted semi-circular areas of high crop loss (and hence high-impact energy density) ranging from 100 to 500 ft (30 to 150 m) in diameter (not wavelength) which may be due to an even smaller scale of hailfall. Such small-scale variations are likely related to frequent reports, at least in Alberta, of more than one burst of hail (Morrow, 1976). Pell (1971) referred to these as "point hailfalls." Barge (personal communication) has identified small-scale radar echo features that are associated with growing cloud towers in the storm mass, and have a typical scale of a few kilometres. Similar small-scale patterns have been referred to by others as "hailcores" (Admiral, 1972).

5 Measurement errors as a function of network density

The question of what network density is required in order to adequately measure hailfall energies is one with particular significance for the evaluation of hail suppression experiments. The answer must clearly depend on what is meant by "adequate." If, for instance, it is desired to compare hailfall patterns on the ground with radar echoes aloft, the spatial resolution of the hailpad network should be commensurate with that of the radar. We have shown, for instance, that with a mean network spacing of half the wavelength of significant variations in the hailfall pattern or greater, these variations cease to be resolved. This is not surprising in view of the aliasing effect, which results in wavelengths shorter than twice the network spacing being "folded" into wavelengths longer than twice the network spacing.

If, on the other hand, one wishes to obtain an accurate estimate of the mean areal energy density of the swath, the required network density can be specified in terms of the inaccuracy that one is prepared to tolerate. Questions of this nature have been examined empirically by Huff (1971) and by Herndon et al. (1973) using dense networks of rain gauges. Further empirical results were obtained by Morgan and Towery (1975), who looked at measurements of crop damage by hail and by Changnon (1968) who examined how the estimated areal extent of damaging hail varied with the measurement network density. In all of these papers the authors assumed the true rainfall or crop damage distributions to be given by measurements made with a high-density network. They then performed Monte Carlo experiments to assess possible errors with other network densities. The disadvantages of this method are that Monte Carlo experiments are tedious and costly and they cannot provide error estimates for network densities greater than those actually used. The method to be described here begins in much the same way by using a high-density net-

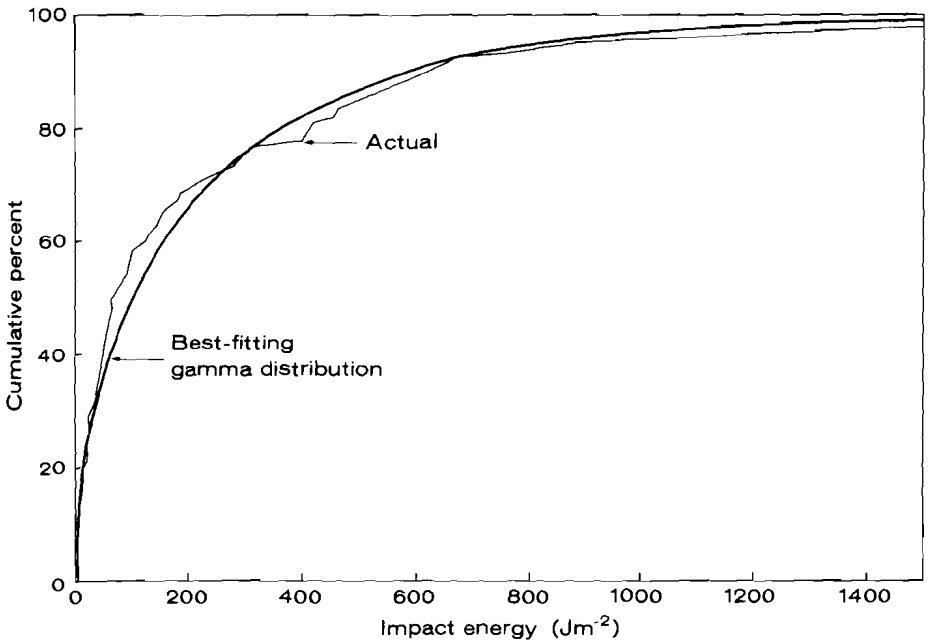


Fig. 12 Cumulative distribution function of energy densities measured over the Northern Network on 16 August 1973, along with the best-fitting gamma distribution.

work to estimate the distribution of hail energy densities. However, we avoid the need for Monte Carlo experiments through the use of elementary probability theory. In so doing, we provide a theoretical basis for the previous empirical work, and a framework for extending the range of its applicability. This approach has been employed with a different objective by Simpson et al. (1973). The basic concept is also to be found in the work of Marshall and Hirschfeld (1953).

In order to begin the analysis, one needs to know the true distribution of areal energy densities in a particular hailswath. This can only be determined by making measurements at all points within the swath. Lacking this information, we turn to the best estimate available, namely the distribution of hail energies measured by the present hailpad network. We will take the hailswath of 16 August 1973 as an example, in order to demonstrate the approach used. Although the entire swath does not lie within the network, it will suffice for an illustration. The cumulative distribution function of the measured energy densities is shown as the jagged curve in Fig. 12. Also shown is the best-fitting gamma distribution, whose parameters were obtained using the method described by Panofsky and Brier (1963). We will assume henceforth that the true distribution function for the energy densities from this swath is the gamma distribution and that the measured distribution is an approximation to it. It is not necessary in what follows, to assume a gamma distribution. Any distribution that provides a good fit to the observed distribution, and for which the distribution of sample means is theoretically determinable, may be used.

The gamma distribution:

$$\Phi(x, \alpha, \beta) = \int_0^x \frac{\xi^{\alpha-1}}{\beta^\alpha \Gamma(\alpha)} e^{-\xi/\beta} d\xi \quad (6)$$

has the property that the means of random samples of size k are also gamma distributed according to $\Phi(x, k\alpha, \beta/k)$.

For the 16 August example, the parameters of the best-fitting gamma distribution are $\hat{\alpha} = 0.5219$ and $\hat{\beta} = 412.5 \text{ J m}^{-2}$, giving a mean $\hat{\mu} = \hat{\alpha}\hat{\beta} = 215.3 \text{ J m}^{-2}$ and standard deviation $\hat{\sigma} = \hat{\alpha}^{\frac{1}{2}}\hat{\beta} = 298.0 \text{ J m}^{-2}$. (The mean and standard deviation of the 66 observations from the regular hailpad network, not including the dense network, are 215.3 J m^{-2} and 316.5 J m^{-2} , respectively.) The mean and standard deviation of the distribution of means for samples of size k is then μ and σ/\sqrt{k} . The central limit theorem requires that as $k \rightarrow \infty$, $\Phi(x, k\alpha, \beta/k)$ must approach a normal distribution function whose mean and standard deviation are also given by μ and σ/\sqrt{k} .

Using these results, the probability that the mean of a random sample of size k be less than a certain multiple of the true mean, $\xi\mu$, say, is just $\Phi(\xi\mu, k\alpha, \beta/k)$. Alternately, $p\%$ of the means of all random samples of size k will lie below $\xi\mu$ if:

$$\Phi(\xi\mu, k\alpha, \beta/k) = \frac{p}{100}. \quad (7)$$

Given p , this equation can be solved for ξ , using tables of the incomplete gamma function (Pearson, 1951). The results of such calculations for the 16 August case, are illustrated in Fig. 13. Since the measured swath area is approximately 410 mi^2 , the x -axis scale can be readily transformed from k to station density, for this case.

For random samples of size 10, that is, ten hailpads within the swath, the graph shows that 95% of the estimates of mean energy density will lie between 0.36μ and 2.03μ , 80% will lie in the range 0.51μ to 1.58μ , and 50% will lie between 0.68μ and 1.25μ . In order to test these predictions a Monte Carlo experiment was performed in which random samples of size 10 were selected (with replacement) from the 66 hailpad observations. The distribution of the resulting means is indicated by the black squares in Fig. 13. The comparison with the theoretical distribution is good, except near the tail. The discrepancy here can probably be ascribed to the small number of samples used to determine the distribution of the means (only 100). The dots at $k = 90$ are given by a normal distribution, illustrating the approximate validity of the central limit theorem in this case even when k is not very great.

Fortunately, samples obtained using an approximately uniformly spaced array of hailpads are not strictly random because there is a certain minimum distance between pads. The spatial dispersion of the hailpad samples will reduce the probability of extreme (i.e. very high or very low) mean values, below that to be expected with completely random samples. Consequently, the error estimates in Fig. 13 must be regarded only as an upper bound. This upper bound will be approached in practice if (a) the distribution of hailpads within the swath is not uniform or (b) the mean spacing of the hailpads is very much

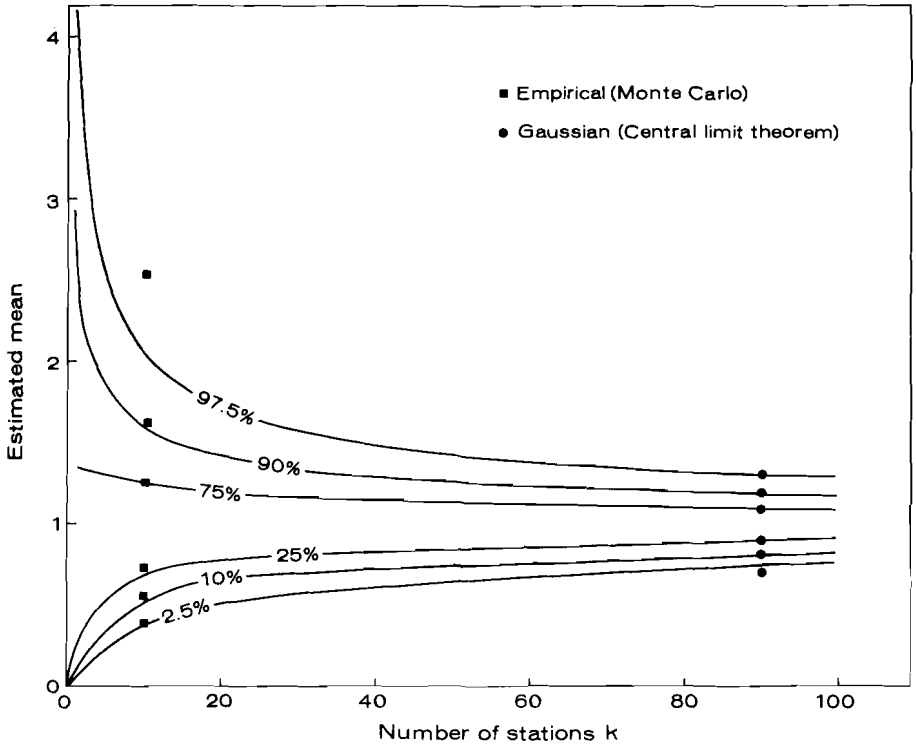


Fig. 13 Probability distribution of the estimated (with k stations) mean energy density of the 16 August 1973 hailswath. The estimated mean is presented as a multiple of the true mean energy density.

larger than the scale of significant spatial variations within the swath.

A further question that may arise is what will be the effect on Fig. 13 of the errors in estimating the true distribution with only 66 pad observations? In a sense this question is irrelevant, since we can *postulate* that a gamma distribution with the given mean and standard deviation is the true distribution function for *some* hailswaths (not necessarily the 16 August one). The fact that the energy distribution from the observed hailswath on 16 August closely fits the assumed gamma distribution, lends some credence to this contention.

5 Conclusions

The 1973 hailpad analysis of 17 storms showed that hailfall patterns are not as sporadic or patchy as many have believed. Part of the 23 August pattern might be termed sporadic, but more than one hailswath was suspected in this case.

Hailpad networks are a viable measurement tool in Alberta, but one must be aware of the limits that a particular network design places on the analysis of any results. This work has provided a means for determining such limits for hailfall.

An approximate relation between impact energy and crop damage has been found. Furthermore the hailpad provides its best measurements of hailfall

over the range of most significant crop damage (impact energies of 50 to 450 J m⁻²). Crop damage estimates are dependent on crop type, soil type, time in the growing season, and so on, and hence they are less reliable than hailpads as a measure of hailfall unless all the relevant agricultural variables can also be measured and taken into account.

Although careful hand analysis of hailpads is a tedious operation, it can be done objectively (Strong, 1974), yielding large amounts of data cheaply. The hailpads of this study cost about \$0.25 each, while the analysis cost was about \$1 per pad. The latter cost could likely be reduced further by means of an automated analysis technique.

Acknowledgments

This work was financed by Alberta Hail Studies of the Alberta Research Council, and by the Atmospheric Environment Service of Canada. Most of it is based on the M.Sc. thesis of one of us (G.S.S.), written while on educational leave from the Atmospheric Environment Service. The authors wish to thank Dr P.W. Summers and Mr J.H. Renick who suggested the project and helped to get it started and Mrs Laura Smith for her suggestions and excellent typing of the manuscript.

List of Symbols

C_D	– drag coefficient for a spherical hailstone
ρ	– average hailstone density
ρ_a	– air density
w_T	– terminal velocity
g	– acceleration of gravity
D_H	– diameter of spherical hailstone
m	– mass of hailstone
D_D	– diameter of hailpad dent
N	– number of hailstones
e_V	– vertical partition of impact energy of a hailstone
e_H	– horizontal partition of impact energy
e_{VT}	– total impact energy (horizontal plus vertical)
W_H	– wind speed
$\Phi(x)$	– gamma distribution functions
α, β	– parameters of the gamma distribution
$\Gamma(\alpha)$	– complete gamma function
k	– sample size

References

- ADMIRAT, P. 1972. Structures fines des chutes de grêle naturelles. In *Recherches sur la prévention de la grêle*. Projet Languedoc Été, 1972. Rapport Tech. No. 14, Décembre, GIEFA.
- BROWNING, K.A. 1964. Airflow and precipitation trajectories within severe local storms which travel to the right of winds. *J. Atmos. Sci.* **21**: 634–9.
- BUTCHBAKER, A.F. 1968. Evaluation of a hail suppression program in southwestern North Dakota. *Proc. 1st National Conf.*

- on Weather Modification, Amer. Meteor. Soc.: 503-12.
- CHANGNON, S.A. JR. 1968. Effect of sampling density on areal extent of damaging hail. *J. Appl. Meteor.* 7: 518-21.
- . 1969. Hail evaluation techniques. Final Report, Part I, Illinois State Water Survey, Urbana, 97 pp.
- . 1970. Hailstreaks. *J. Atmos. Sci.* 27: 109-25.
- and N.A. BARRON. 1971. Quantification of crop-hail losses by aerial photography. *J. Appl. Meteor.* 10: 86-96.
- and N.G. TOWER. 1972. Studies of hail data in 1970-72. Final Report, Illinois State Water Survey, Urbana, 28 pp.
- CHISHOLM, A.J. and M. ENGLISH. 1973. *Alberta Hailstorms*. Meteorological Monographs 14, No. 36. Boston: Amer. Meteor. Soc., 98 pp.
- DECKER, F.W. and L.D. CALVIN. 1961. Hail-fall of 10 September 1959 near Medford, Oregon. *Bull. Amer. Meteor. Soc.* 42: 475-80.
- HAGEN, L. and A.F. BUTCHBAKER. 1967. Climatology of hailstorms and evaluation of cloud seeding for hail suppression in Southwestern North Dakota. *Proc. 5th Conf. on Severe Local Storms*, Amer. Meteor. Soc., St. Louis: 336-47.
- HERNDON, A.; W.L. WOODLEY; A.H. MILLER; A. SAMET; and H. SENN. 1973. Comparison of gage and radar methods of convective precipitation measurement. *NOAA Tech. Mem.* ERL OD-18.
- HUFF, F.A. 1971. Evaluation of precipitation records in weather modification experiments. *Advances in Geophysics* 15: 59-134. New York and London: Academic Press.
- LOZOWSKI, E.P. and A.G. BEATTIE. 1975. Field measurements of hailstone aerodynamics. Unpublished paper presented at the 9th Annual Congress Can. Meteor. Soc., May 1975, Vancouver, B.C.
- and G.S. STRONG. 1975. On the calibration of hailpads. Unpublished paper presented at the 9th Annual Congress Can. Meteor. Soc., May 1975, Vancouver, B.C.
- MARSHALL, J.S. and W. HITSCHFELD. 1953. Interpretation of the fluctuating echo from randomly distributed scatterers. Pt. 1. *Can. J. of Physics* 31: 962-94.
- MORGAN, G.M. JR. and N.G. TOWER. 1974. Micro-scale studies of surface hailfall. Final Report on Subcontract No. NCAR 25-73 for the University Corp. for Atmospheric Research, Illinois State Water Survey, Urbana, 35 pp.
- . 1975. Small-scale variability of hail and its significance for hail prevention experiments. *J. App. Meteor.* 14: 763-70.
- MORROW, T.M. 1976. Time variation of Alberta hailfalls. Unpublished M.Sc. thesis, Div. of Meteorology, Univ. of Alberta.
- NEWTON, C.W. and S. KATZ. 1958. Movement of large convective rainstorms in relation to winds aloft. *Bull. Amer. Meteor. Soc.* 39: 129-36.
- PANOFSKY, H.A. and G.W. BRIER. 1963. *Some applications of statistics to meteorology*. University Park: Pennsylvania State Univ. Press.
- PEARSON, K. 1951. *Tables of the incomplete gamma function*. Cambridge Univ. Press, 164 pp.
- PELL, J. 1971. Variations with time of six Alberta hail parameters. *Proc. 7th Conf. on Severe Local Storms*, Amer. Meteor. Soc., Kansas City: 226-33.
- RENICK, J.H. 1971. Radar reflectivity profiles of individual cells in a persistent multicellular Alberta hailstorm. *Proc. 7th Conf. on Severe Local Storms*, Amer. Meteor. Soc., Kansas City: 63-70.
- SCHLEUSENER, R.A. and P.C. JENNINGS. 1960. An energy method for relative estimates of hail intensity. *Bull. Amer. Meteor. Soc.* 41: 372-7.
- SIMPSON, J.; J.C. EDEN; A. OLSEN; and J. PEZIER. 1973. On the use of gamma functions and Bayesian analysis in evaluating Florida cumulus seeding results. *NOAA Tech. Mem.* ERL OD-15.
- STRONG, G.S. 1974. Objective measurement of Alberta hailfall. M.Sc. thesis, Univ. of Alberta, 182 pp.
- SUMMERS, P.W. and L. WOJTIW. 1971. The economic impact of hail damage in Alberta, Canada and its dependence on various hailfall parameters. *Proc. 7th Conf. on Severe Local Storms*, Amer. Meteor. Soc., Kansas City: 158-63.

NOTES AND CORRESPONDENCE

GLOBAL FLOW-VISUALIZATION

OR

“THEODORE VON KÁRMÁN WINS AGAIN!”

H.W. Teunissen

*Atmospheric Environment Service, 4905 Dufferin St,
Downsview, Ontario M3H 5T4*

[Original manuscript received 18 November 1976; in revised form 17 January 1977]

In 1911–12, the brilliant scientist–experimentalist–analyst Theodore von Kármán (1881–1963) developed his now-famous theory of the “vortex street” (Goldstein, 1938; Schlichting, 1968) in which a circularly cylindrical body, when exposed to a fluid flowing perpendicular to its length, alternately sheds vortices from opposite sides of it. This phenomenon is familiar to many of us as the cause of the “humming” of telephone or power lines in high winds, a sound which is usually referred to as “Aeolian tones.” It is extremely important in that it can have very destructive effects on stacks and chimneys and the like and also, to a lesser extent, on suspended cables.

Since von Kármán’s original work, considerable research has been conducted into the theoretical and experimental aspects of vortex shedding from cylinders (e.g. Roshko, 1954a, 1954b, and 1961; Schlichting, 1968; Wooton and Scruton, 1971). Although the phenomenon is still not perfectly understood, many interesting results have been obtained. For example, it was originally thought that organized vortex shedding occurs over only a very limited range of Reynolds number ($Re \equiv \rho V D / \mu$; see Fig. 2 for definition of symbols). Laboratory results have shown, however, that it exists to a Reynolds number of at least 10^7 (Roshko, 1961), and there is no reason to believe that this value is an upper limit. It is virtually impossible to produce higher values of Re in the laboratory, however, so results in this range have remained largely unavailable. Another result has been the determination of the frequency with which the vortices are shed from the body. This frequency is usually expressed in terms of a Strouhal number, which is defined by $St = fD/V$. The Strouhal shedding frequency appears to be about 0.27 for circular cylinders at high Re , decreasing to about 0.20 for lower values of Re and 0.10–0.25 for non-circular cross-sections.

The purpose of this brief note is to focus attention on the photograph of Fig. 1 in light of von Kármán’s original two-dimensional vortex shedding theory and some of the more recently observed aspects of the phenomenon. The photograph displays a splendid example of the natural occurrence of a form of vortex shedding on a Reynolds number scale ($Re \sim 10^{10}$) far greater than



Fig. 1 Photograph of the flow of air past Isla de Guadalupe (Mex.) off the coast of Baja California, obtained at the Atmospheric Environment Service on 25 Aug. 1976 (NOAA 5, Orbit #334). Mist and clouds provide the medium needed to make the flow structure visible.

can be achieved in typical laboratory experiments. It was obtained in the Atmospheric Environment Service Satellite Data Laboratory and shows the flow of air past Isla de Guadalupe off the coast of Baja California. While such photographs have become fairly familiar in recent years (e.g. Bayliss, 1976), they remain a pleasing reminder of the existence of the phenomenon on a global scale and of the flow-visualization capabilities that are provided by satellite photography.

We can examine some of the relevant parameters of the present flow by using dimensional information from the photograph and wind data from the island for this date. The flow is reconstructed in Fig. 2 and appropriate values are given. Using these data, we obtain a Reynolds number of 5.2×10^9 and a Strouhal number of 0.15. The latter value certainly agrees favourably with

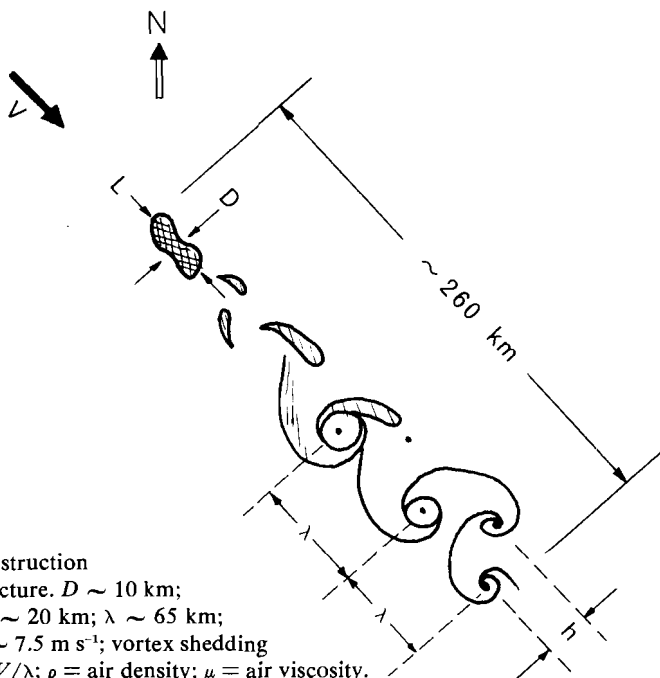


Fig. 2 Reconstruction of the flow structure. $D \sim 10$ km; $L \sim 35$ km; $h \sim 20$ km; $\lambda \sim 65$ km; wind speed $V \sim 7.5$ m s⁻¹; vortex shedding frequency $f = V/\lambda$; ρ = air density; μ = air viscosity.

those quoted above, especially when it is kept in mind that this full-scale case represents a three-dimensional flow over a mountain that is 1300 m high, as opposed to a controlled two-dimensional flow past a cylinder!

Finally, it is interesting to calculate the value of h/λ for this flow (see Fig. 2). In his original theory, von Kármán concluded that the vortex street would remain stable only if this ratio were equal to 0.28. From the photograph, we obtain a value of $h/\lambda \sim 0.3!$

You win again, Dr von Kármán!

Acknowledgment

The author wishes to thank Dr David Surry of the University of Western Ontario for critically reviewing this note.

References

- BAYLISS, P. 1976. *Weather* **31**: 346.
- GOLDSTEIN, S., ed. 1938. *Modern developments in fluid dynamics*. Volume II. Oxford University Press.
- ROSHKO, A. 1954a. *On the development of turbulent wakes from vortex streets*. NACA Report 1191.
- . 1954b. *On the drag and shedding frequency of two-dimensional bluff bodies*. NACA Tech. Note 3169.
- . 1961. Experiments on the flow past a circular cylinder at very high Reynolds number. *J. Fluid Mech.* **10**: 345–56.
- SCHLICHTING, A. 1968. *Boundary-layer theory*. McGraw-Hill.
- WOOTON, L.R. and SCRUTON, C. 1971. *Aerodynamic stability*. Paper 5: The modern design of wind sensitive structures. London: CIRIA.

BOOK REVIEWS

ADVANCES IN GEOPHYSICS, volume 19. H.E. Landsberg and J. van Meighem, editors. Academic Press, 1976, 312 pp., hardcover, \$29.00.

This volume in the series *Advances in Geophysics* consists of three articles:

"Precipitation augmentation from cumulus clouds and systems: scientific and technological foundations, 1975," by Joanne Simpson;

"The properties of atmospheric aerosol particles as functions of the relative humidity at thermodynamic equilibrium with the surrounding moist air," by Gottfried Hänel; and

"A three-dimensional model for the numerical simulation of estuaries," by Erique A. Caponi.

Only the first two contributions are reviewed here.

Simpson's article is divided into two main chapters the first of which deals with the scientific basis, and the second with the technological basis for the modification of cumulus clouds. The author has tended to present a broad overview of cloud physics rather than to focus on the important advances and gaps in the basis of cumulus precipitation augmentation. Although the title is very specific, the article is in fact very general. This is particularly so in the first part of the chapter on the scientific basis which deals with microphysics. In less than six pages the whole gamut of cloud microphysics is briefly discussed, starting with cloud condensation nuclei and ending with cloud electrification. Needless to say, none of the almost one-dozen topics is treated in detail, and yet neither are most of them related in the article to precipitation augmentation theories. I believe the article would have been much more useful if greater emphasis had been placed on the specific relationships of cloud physics to cumulus modification. The section on microphysics does single out some aspects for special attention, such as the bimodality of some cloud droplet spectra and the often observed ice crystal-nucleus concentration discrepancy, and the related experiments on splinter production by riming. The next section on cumulus dynamics and modelling contains a good description of the historical development of one-dimensional models, as well as their successes and failings. The role of these models in the design and evaluation of dynamic seeding experiments in Florida is, naturally, particularly well documented. The severe limitations of one-dimensional models are recognized and mention is made, together with a healthy note of caution, of some of the advances in the formulation of two- and three-dimensional models. The chapter closes with an interesting discussion of various aspects of cloud interactions, downwind effects, and interactions with the boundary layer.

The chapter on the assessment of the technological basis for cumulus modification begins with a critical overview of the various silver iodide delivery systems. It is here that the author points out that, among other gaps in our knowledge, neither the optimum amount nor the optimum location of the seeding agent is known. These are hardly technological problems and should have been discussed in the previous chapter. Brief mention is made of tracers, trace detection techniques, organic nucleants, and warm cloud modification. This section is followed by one on measuring systems, in which the instrumentation required to measure precipitation and to monitor the microphysical and dynamical changes in the cloud are reviewed. The final section discusses the role of statistics on the design and analysis of seeding experiments.

This article assimilates a great deal of information from many different sources into a form convenient as a starting point for further investigation into specific aspects of cumulus modification. Its long list of references will be particularly useful. Nevertheless, I feel that this was an opportunity missed. Professor Simpson has had extensive involvement with cloud-seeding experiments, and is in a particularly advantageous position to point out the

predominant foundations of current cumulus modification experiments and programs, and the important gaps in these foundations. Consequently a more selective and detailed approach to the topic would have been even more valuable.

Hänel has written a very impressive treatise on the properties of atmospheric aerosols as functions of relative humidity. He first develops equations relating the mass, density and complex refractive index of single aerosol particles to relative humidity, and then modifies these equations to describe the functional dependence on relative humidity of these properties for aerosol samples. The author then lists the measurements required to calculate the above properties from the theory as well as the required accuracy of the measurements. The article continues with brief descriptions, and discussions of the principles of the sophisticated apparatus built by Hänel to carry out the measurements to the necessary accuracy.

Measurements of the properties of six different aerosol samples are reported, followed by application of the theory to deduce the humidity dependence of the mean equivalent radius, mean density, and mean refractive index, as well as geometric cross-sections, extinction and absorption coefficients for radiation at a number of wavelengths between 0.3 and 12 μm . Finally as examples of applications of the results the author discusses the estimate of visible range, the ratio of extinction coefficient to aerosol mass, and the single scattering albedo – all as functions of humidity.

The presentation of theory and data allowing for the first time the reliable calculation of the humidity dependence of many of the properties of aerosols is an important achievement. The continuity of the material, including theory, measurements, and application of the theory allows increased appreciation of each aspect of the work. The development of the theory is presented clearly, as is its application. The numerous results are in useful tabular form. In the opinion of this reviewer this article will be of considerable interest and value to most of those concerned with the properties of atmospheric aerosols.

H.G. Leighton
McGill University
Montreal

ANNOUNCEMENTS

GATE Data Available

During the GARP Atlantic Tropical Experiment, GATE, a large amount of meteorological and oceanographical data was collected. These data have now been processed and validated and are available to users at nominal cost. The types of Canadian data available are:

- 1 Hourly surface meteorological observations.
- 2 Upper air data of winds, temperatures and humidity.
- 3 Hourly and ten-minute values of surface radiation components.
- 4 Tethered balloon boundary layer measurements to 1 km.
- 5 Precipitation data including digital radar data.
- 6 Wind profiles from surface boom.
- 7 CTD, XBT, current meter and thermistor chain oceanographic data.

Validated data from all nations participating in GATE are also available. Interested scientists are encouraged to take advantage of this valuable data set.

For further information please contact either The National Processing Centre or Dr R.J. Polavarapu at Atmospheric Environment Service, 4905 Dufferin Street, Downsview, Ontario M3H 5T4.

FORMULE D'ADHÉSION

(Lettres moulées, s.v.p.)

Membre NOM

ou PRÉNOM(S)

Membre-étudiant ADRESSE

TITRE, RANG, DÉCORATIONS, DEGRÉS OU QUALIFICATION

PROFESSIONNELLE

OCCUPATION

(Pour registres seulement. L'étudiant doit inscrire le nom de son université et la date où il finira ses études)

Membre de soutien NOM OU RAISON SOCIALE

ADRESSE

Type de Membre J'aimerais devenir membre de la Société météorologique du Canada à compter du 1^{er} janvier 19....., et recevoir toutes les publications de la Société par la suite. Vous trouverez ci-inclus un chèque de \$ libellé à *La Société météorologique du Canada*.

Signature du candidat

Envoyer cette formule d'adhésion au:	Cotisation annuelle, pour 1977.
Secrétaire	Membre \$20.00
Société météorologique du Canada	Membre étudiant \$ 5.00
a/s Département de géographie	Membre de soutien \$60.00 (min.)
Université Simon Fraser	
Burnaby, Colombie Britannique	
V5A 1S6	

MEMBERSHIP APPLICATION FORM

(Please write in Block Letters)

*General
or
Student
Member* SURNAME

GIVEN NAMES

PERMANENT ADDRESS

.....

TITLE, RANK, DECORATIONS, DEGREES OR PROFESSIONAL
QUALIFICATIONS

OCCUPATION

(for record purposes only; if student, indicate university and
year studies will be completed)

*Sustaining
Member* NAME OR AGENCY

BUSINESS ADDRESS

.....

*Membership
Status
Required* Please enroll me as a member
of the Canadian Meteorological Society effective January 1,
19....., to receive all publications issued by the Society from
that date. I attach a cheque for \$ payable to the
Canadian Meteorological Society.

Signature of Applicant

Mail completed application forms to:	CMS dues for 1977.
Corresponding Secretary	General Member \$20.00
Canadian Meteorological Society	Student Member \$ 5.00
c/o Dept. of Geography	Sustaining Member \$60.00 (min.)
Simon Fraser University	
Burnaby, B.C.	
V5A 1S6	

INFORMATION FOR AUTHORS

Editorial policy. *Atmosphere* is a medium for the publication of the results of original research, survey articles, essays and book reviews in all fields of atmospheric science. It is published quarterly by the CMS with the aid of a grant from the Canadian Government. Articles may be in either English or French. Contributors need not be members of the CMS nor need they be Canadian; foreign contributions are welcomed. All contributions will be subject to a critical review before acceptance. Because of space limitations articles should not exceed 16 printed pages and preferably should be shorter.

Manuscripts should be submitted to: *Atmosphere*, Dept. of Meteorology, McGill University, 805 Sherbrooke St W., Montreal, Quebec, H3A 2K6. Three copies should be submitted, typewritten with double spacing and wide margins. Heading and sub-headings should be clearly designated. A concise, relevant and substantial abstract is required.

Tables should be prepared on separate sheets, each with concise headings.

Figures should be provided in the form of three copies of an original which should be retained by the author for later revision if required. A list of legends should be typed separately. Labelling should be made in generous size so that characters after reduction are easy to read. Line drawings should be drafted with India ink at least twice the final size on white paper or tracing cloth. Photographs (halftones) should be glossy prints at least twice the final size.

Units. The International System (SI) of metric units is preferred. Units should be abbreviated only if accompanied by numerals, e.g., "10 m," but "several metres."

Footnotes to the text should be avoided.

Literature citations should be indicated in the text by author and date. The list of references should be arranged alphabetically by author, and chronologically for each author, if necessary.

RENSEIGNEMENTS POUR LES AUTEURS

Politique éditoriale. *Atmosphère* est un organe de publication de résultats de recherche originale, d'articles sommaires, d'essais et de critiques dans tous les domaines des sciences de l'atmosphère. Il est publié par la SMC à l'aide d'une subvention accordée par le gouvernement canadien. Les articles peuvent être en anglais ou en français. Il n'est pas nécessaire que les auteurs soient membre de la SMC; les contributions étrangères sont les bienvenues. A cause des limitations d'espace les articles ne doivent pas dépasser 16 pages dans le format final. Tout article sera soumis à un critique indépendant avant d'être accepté.

Les manuscrits doivent être envoyés à: *Atmosphère*, Dép. de météorologie, L'Université McGill, 805 Sherbrooke O., Montréal, Québec, H3A 2K6. Ils doivent être soumis en trois exemplaires dactylographiés à doubles interlignes avec de larges marges. Les titres et sous-titres doivent être clairement indiqués. Chaque article doit comporter un résumé qui soit concis, pertinent et substantiel.

Les tableaux doivent être préparés et présentés séparément accompagnés d'un titre concis et d'un numéro.

Les graphiques doivent être présentés en trois copies dont les originaux devraient être conservés par l'auteur au cas où ils seraient nécessaire de les reviser. Une liste des légendes des graphiques doit être dactylographiée séparément. L'étiquetage doit être de grand format de façon à ce qu'il soit facilement lisible après réduction du format. Le traçage des lignes doit s'effectuer au moyen d'encre de chine en doublant, au moins, le format final, le tout sur papier blanc ou sur papier à calquer et identifié adéquatement. Les photographies (demi-teintes) devraient être présentées sur épreuves glacées au double du format final.

Les unités. Le Système International (SI) d'unités métriques est préférable. Les unités devraient être abrégées seulement lorsqu'elles sont accompagnées de nombres, ex: "10m," mais "plusieurs mètres."

Les notes de renvoi au texte doivent être évitées.

Les citations littéraires doivent être indiquées dans le texte selon l'auteur et la date. La liste des références doit être présentée dans l'ordre alphabétique, par auteur et, si nécessaire, dans l'ordre chronologique pour chaque auteur.

The Canadian Meteorological Society / La Société météorologique du Canada

The Canadian Meteorological Society came into being on January 1, 1967, replacing the Canadian Branch of the Royal Meteorological Society, which had been established in 1940. The Society exists for the advancement of Meteorology, and membership is open to persons and organizations having an interest in Meteorology. At nine local centres of the Society, meetings are held on subjects of meteorological interest. *Atmosphere* as the scientific journal of the CMS is distributed free to all members. Each spring an annual congress is convened to serve as the National Meteorological Congress.

Correspondence regarding Society affairs should be directed to the Corresponding Secretary, Canadian Meteorological Society, c/o Dept. of Geography, Simon Fraser University, Burnaby 2, B.C.

There are three types of membership – Member, Student Member and Sustaining Member. For 1977 the dues are \$20.00, \$5.00 and \$60.00 (min.), respectively. The annual Institutional subscription rate for *Atmosphere* is \$15.00.

Correspondence relating to CMS membership or to institutional subscriptions should be directed to the University of Toronto Press, Journals Department, 5201 Dufferin St., Downsview, Ontario, Canada, M3H 5T8. Cheques should be made payable to the University of Toronto Press.

La Société météorologique du Canada a été fondée le 1^{er} janvier 1967, en remplacement de la Division canadienne de la Société royale de météorologie, établie en 1940. Cette société existe pour le progrès de la météorologie et toute personne ou organisation qui s'intéresse à la météorologie peut en faire partie. Aux neuf centres locaux de la Société, on peut y faire des conférences sur divers sujets d'intérêt météorologique. *Atmosphère*, la revue scientifique de la SMC, est distribuée gratuitement à tous les membres. A chaque printemps, la Société organise un congrès qui sert de Congrès national de météorologie.

Toute correspondance concernant les activités de la Société devrait être adressée au Secrétaire-correspondant, Société météorologique du Canada, Département de Géographie, L'Université Simon Fraser, Burnaby 2, B.C.

Il y a trois types de membres: Membre, Membre-étudiant, et Membre de soutien. La cotisation pour 1977 est de \$20.00, \$5.00 et \$60.00 (min.) respectivement. Les institutions peuvent souscrire à *Atmosphère* au coût de \$15.00 par année.

La correspondance concernant les souscriptions à la SMC ou les souscriptions des institutions doit être envoyée aux Presses de l'Université de Toronto, Département des périodiques, 5201 rue Dufferin, Downsview, Ontario, Canada, M3H 5T8. Les chèques doivent être payables aux Presses de l'Université de Toronto.

Council / Conseil d'administration 1976-77

President/Président – J.E. Hay
Vice President/Vice-Président – K.F. Harry
Past President/Président sortant –
P.E. Merilees
Corresponding Secretary/Secrétaire-correspondant –
R.B. Sagar
Treasurer/Trésorier – D.G. Schaefer
Recording Secretary/Secrétaire d'assemblée – L.E. Parent

Councillors-at-large/Conseillers
– M.G. Ferland, D.B. Fraser,
A.D.J. O'Neill
Chairmen of Local Centres/Présidents des centres
Oceanography Division/Division
d'océanographie:
Chairman/Président – D.M. Farmer
Secretary/Secrétaire – P.H. LeBlond
Councillors/Conseillers – E.P. Jones,
B. Sundby

ATMOSPHERE

Editor/Rédacteur – J. Derome
Associate Editors/Rédacteurs adjoints – C. East, J.B. Gregory, W. Gutzman, P.H. LeBlond,
R. List, C.L. Mateer, G.A. McBean, D.N. McMullen, P.E. Merilees, R.R. Rogers, V.R.
Turner, R.E. Thomson, E.J. Truhlar, E. Vowinckel
Technical Editor/Editeur technique – L. Burton

Sustaining Members/Membres de soutien – Air Canada. – MacLaren Atlantic Ltd.